iScience

CellPress

Article

# AMP-Activated Protein Kinase Is Essential for the Maintenance of Energy Levels during Synaptic Activation

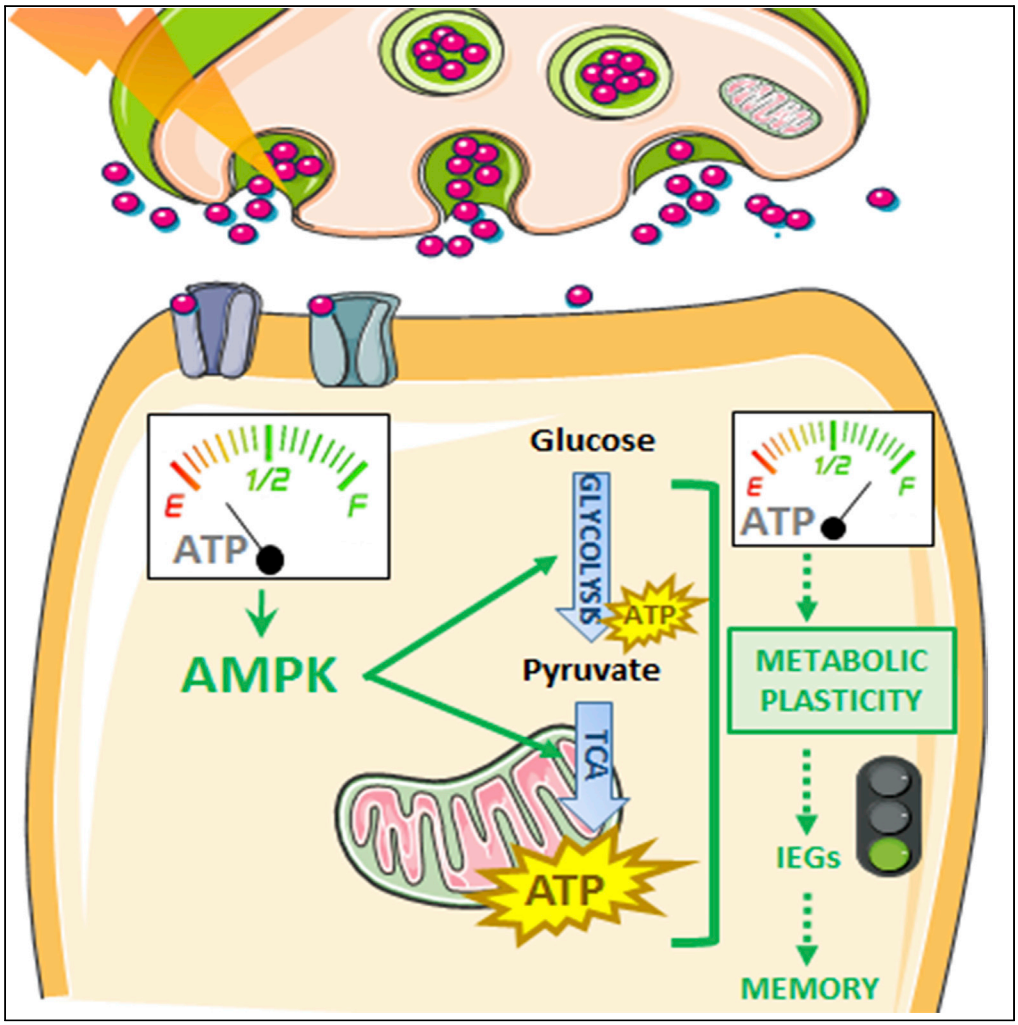


Claudia Marinangeli, Sébastien Didier, Tariq Ahmed, ..., Luc Buée, Jérôme Kluza, Valérie Vingtdeux

valerie.vingtdeux@inserm.fr

## HIGHLIGHTS

AMPK is rapidly activated following synaptic activation

AMPK stimulates neuronal glycolysis and oxidative respiration, i.e., metabolic plasticity

Metabolic plasticity ensures the expression of IEGs and long-term memory formation

AMPK deregulation, as in Alzheimer disease, prevents metabolic plasticity response

Marinangeli et al., iScience 9, 1–13
November 30, 2018 
https://doi.org/10.1016/j.isci.2018.10.006

iScience

CellPress

Article

# AMP-Activated Protein Kinase Is Essential for the Maintenance of Energy Levels during Synaptic Activation

Claudia Marinangeli,[1] Sébastien Didier,[1] Tariq Ahmed,[2,3,4] Raphaelle Caillerez,[1] Manon Domise,[1] Charlotte Laloux,[5] Séverine Bégard,[1] Sébastien Carrier,[1] Morvane Colin,[1] Philippe Marchetti,[1] Bart Ghesquière,[6] Detlef Balschun,[2,3] Luc Buée,[1] Jérôme Kluza,[1] and Valérie Vingtdeux[1,7,*]

## SUMMARY

**Although the brain accounts for only 2% of the total body mass, it consumes the most energy. Neuronal metabolism is tightly controlled, but it remains poorly understood how neurons meet their energy demands to sustain synaptic transmission. Here we provide evidence that AMP-activated protein kinase (AMPK) is pivotal to sustain neuronal energy levels upon synaptic activation by adapting the rate of glycolysis and mitochondrial respiration. Furthermore, this metabolic plasticity is required for the expression of immediate-early genes, synaptic plasticity, and memory formation. Important in this context, in neurodegenerative disorders such as Alzheimer disease, dysregulation of AMPK impairs the metabolic response to synaptic activation and processes that are central to neuronal plasticity. Altogether, our data provide proof of concept that AMPK is an essential player in the regulation of neuroenergetic metabolic plasticity induced in response to synaptic activation and that its deregulation might lead to cognitive impairments.**

## INTRODUCTION

Although the brain accounts for only 2% of the total body mass, it is one of the most energy-consuming organs, requiring up to 20% of the oxygen and 25% of the glucose metabolized by the body. These substrates are converted to ATP through glycolysis and oxidative phosphorylation, the latter taking place in mitochondria. Hence, around 20% of the ATP produced in the body is devoted to the brain. Importantly, brain functions depend on an adequate energy supply. Indeed, reducing the brain supply of glucose or oxygen even for short periods leads to severe brain damage, as observed following ischemic stroke. Numerous reports support a role for glucose as a potent modulator of learning and memory, including behavioral tasks, in both humans and rodents. Indeed, both peripheral and direct central glucose administration enhances cognitive processes (Gold, 1995). Similarly, astrocytes-derived lactate, the end product of glycolysis, was reported to be necessary for the formation of long-term memory (Suzuki et al., 2011). Consistent with these observations, brain imaging approaches are based on the detection of signals that are directly related to energy supply and use. For instance, positron emission tomography (PET) reveals changes in cerebral blood flow, glucose uptake, and oxygen consumption according to the tracer that is used. These imaging approaches have been instrumental in demonstrating that brain activity is coupled to increased energy availability and consumption. Further studies have demonstrated that 85% of the energy required by the brain is used by neurons and is devoted to glutamatergic transmission (Attwell and Laughlin, 2001; Harris et al., 2012).

Failure to maintain proper energy levels in the brain also leads to neurodegeneration. The main neurodegenerative diseases are characterized by dysregulations of energy metabolism (Ferreira et al., 2010). For instance, Alzheimer disease (AD) is characterized by mitochondrial dysfunctions (Lin and Beal, 2006) and early glucose hypometabolism (Mosconi, 2005). Of note, [$^{18}$F] fluorodeoxyglucose (FDG)-PET, a marker for glucose utilization, was recently described as being the most accurate biomarker for AD. Indeed, FDG-PET allowed to correctly differentiate subjects who progressed to AD or other dementia from those who remained stable or reverted to normal cognition (Caminiti et al., 2018). Finally, although these metabolic impairments were proposed to play a causative role in disease pathogenesis, their causes and consequences remain to be established.

[1]Univ. Lille, Inserm, CHU-Lille, UMR-S1172, Jean-Pierre Aubert Research Centre, Bâtiment Biserte, Place de Verdun, Lille 59045, France

[2]Brain & Cognition, Faculty of Psychology and Educational Sciences, KU Leuven, Leuven, Belgium

[3]Leuven Research Institute for Neuroscience & Disease (LIND), KU Leuven, Leuven, Belgium

[4]Neurological Disorders Research Center, Qatar Biomedical Research Institute (QBRI), Hamad Bin Khalifa University, Doha, Qatar

[5]Univ. Lille, Lille Neurosciences, SFR DN2M, Lille 59000, France

[6]VIB Center for Cancer Biology, KU Leuven, Department of Oncology, Leuven 3000, Belgium

[7]Lead Contact

*Correspondence: valerie.vingtdeux@inserm.fr

https://doi.org/10.1016/j.isci.2018.10.006

One of the most important cell energy sensors and regulators is the AMP-activated protein kinase (AMPK). AMPK is a serine/threonine protein kinase composed of three subunits. It possesses one catalytic subunit alpha and two regulatory subunits beta and gamma. The gamma subunit holds adenine-nucleotide-binding sites that allow the sensing of intracellular levels of AMP, ADP, and ATP. Consequently, any energetic stress that will modify the intracellular AMP/ATP ratio will enhance the activation of AMPK (Xiao et al., 2007). The activation of AMPK requires its phosphorylation on threonine 172 within its catalytic alpha subunit. Two main kinases were reported to fulfill this role, the liver kinase B1, which is thought to be constitutively activated and involved in AMPK phosphorylation in energy stress conditions (Hawley et al., 2003; Woods et al., 2003), and the $Ca^{2+}$/calmodulin-dependent protein kinase kinase-beta (CaMKKβ), whose activation is dependent on intracellular calcium levels (Hawley et al., 2005). AMPK is highly expressed in the brain, and in particular, in neurons. Interestingly, several studies have reported an over-activation of neuronal AMPK in the brain of patients with AD (Vingtdeux et al., 2011), Parkinson disease (Jiang et al., 2013), and Huntington disease (Ju et al., 2011), thus supporting the defective metabolism hypothesis in these disorders (Domise and Vingtdeux, 2016).

Although it is obvious that brain energy metabolism must be tightly regulated to sustain neuronal function and cognition, the molecular mechanisms involved in this regulation remain poorly understood. In particular, how neurons meet their energy demand to sustain synaptic transmission remains to be established. In this study, we assessed the possibility that AMPK might play a critical role in the regulation of energy metabolism in neurons in response to their activation.

## RESULTS

### AMPK Is Stimulated following Synaptic Activation

To assess the molecular pathways involved in neuronal energy level maintenance, we used bicuculline and 4-aminopyridine (Bic/4-AP) to induce synaptic release of glutamate in differentiated primary neurons. This well-established protocol (Hardingham et al., 2002; Hoey et al., 2009) is known to preferentially induce glutamatergic neurotransmission that we will refer to hereafter as synaptic activation (SA). To validate the efficiency of this protocol in our model, we first assessed the activation status of a signaling pathway known to be activated following SA, the MAPK pathway. SA induction in 15 days *in vitro* differentiated mouse primary neurons led to a rapid phosphorylation of the main MAPK pathway components, ERK, RSK, MSK, and MEK, which are representative of this signaling pathway activation (Figure S1A). In addition, blockade of glutamatergic N-methyl-D-aspartate (NMDA) and α-amino-3-hydroxy-5-methyl-4-isoxazolepropionic acid (AMPA) receptors by the specific inhibitors MK-801 and NBQX, respectively, completely abolished the activation of ERK, confirming that MAPK activation is dependent on the stimulation of glutamate receptors (Figure S1B). Together, these results confirm the validity of the SA protocol in our model. To allow a more general screening of the signaling pathways activated following SA we used a kinase array approach. After 5 min Bic/4-AP stimulation, we detected an increase in the phosphorylation status of ERK, MSK, and CREB, as expected from our previous data (Figures 1A, 1B, and 1E). Interestingly, an increase in the phosphorylation levels of AMPK was also observed following Bic/4-AP treatment. AMPK activation was further assessed by western blot using phospho-specific antibodies directed against the AMPK-$Thr^{172}$ epitope, which is a prerequisite for AMPK activity, and acetyl-CoA carboxylase (ACC)-$Ser^{79}$, a direct AMPK target (Figures 1G–1I). Following SA, we observed a rapid phosphorylation of AMPK and ACC, thus demonstrating that the AMPK signaling pathway was activated (Figures 1G–1I). This activation was also dependent on glutamate receptor activation since their inhibition significantly reduced AMPK activation (Figures S1B–S1D). Given that SA leads to intracellular calcium influx and that AMPK was reported to be phosphorylated by the calcium-dependent protein kinase CaMKKβ in neuronal cells, we used the CaMKKβ-specific inhibitor STO-609 to address this possibility. However, our results showed that in our model CaMKKβ was not responsible for the SA-induced AMPK activation (Figure S2), thus strongly suggesting that AMPK phosphorylation was not related to intracellular calcium levels. Since SA is a very energetic process, it is likely that AMPK activation might be related to changes in ATP levels. To assess the importance of energy level maintenance for the signaling pathways induced by SA, primary neurons were pre-treated with a combination of oligomycin, an ATP synthase inhibitor, and 2-deoxy-D-glucose, a glycolysis inhibitor (Oligo/2-DG) to deplete intracellular ATP (Figure 1F). In these conditions of energy depletion, SA failed to activate the MAPK signaling pathway (Figures 1C–1E). However, AMPK activity was increased in both conditions (Figures 1C–1E). Altogether, our data show that the activation of the MAPK signaling pathway by SA is contingent upon intracellular energy levels, suggesting a role of AMPK in their regulation.

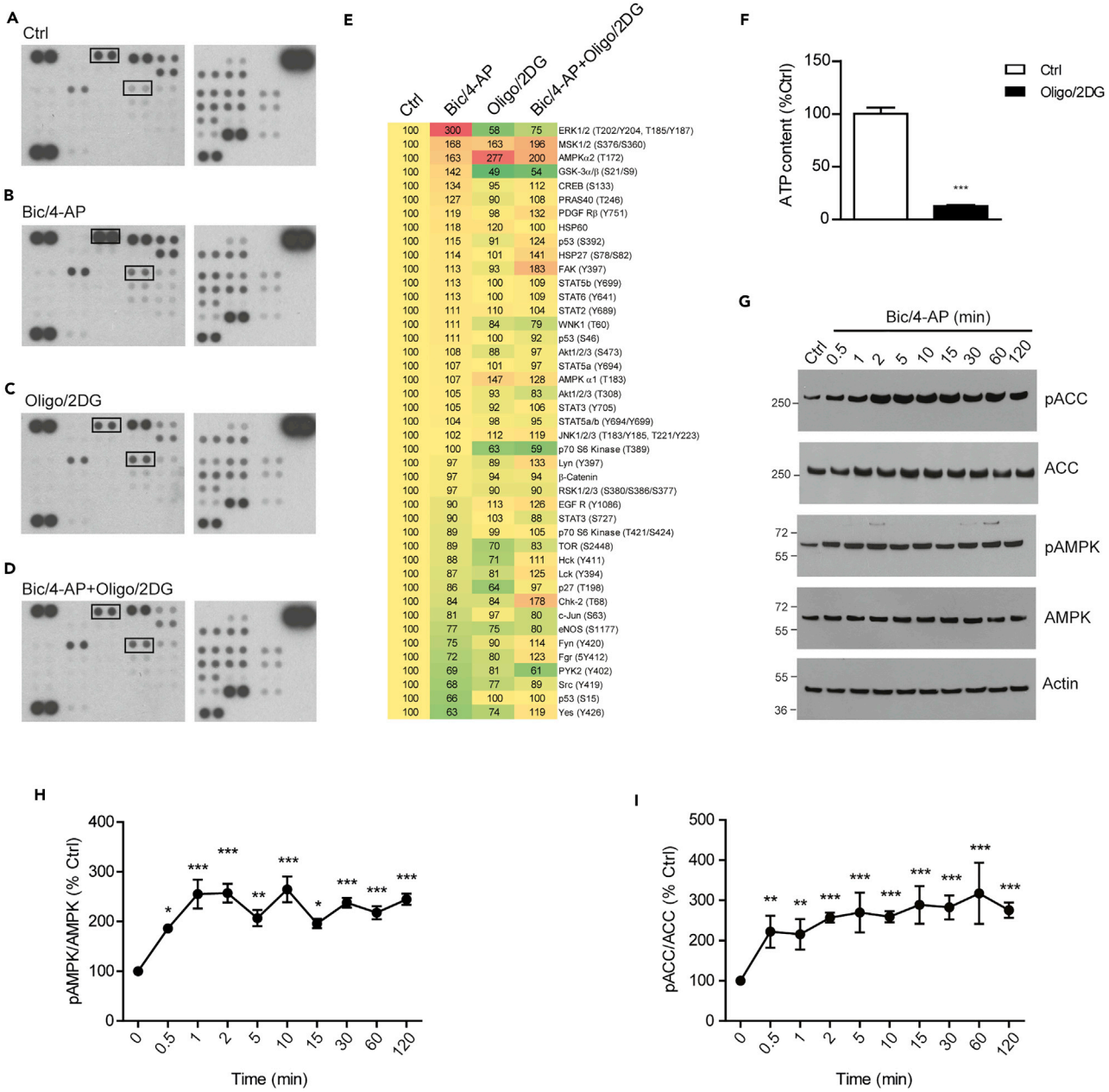


**Figure 1. AMPK Is Activated upon Synaptic Activation**

(A–D) 15 days *in vitro* (DIV) differentiated primary neurons were stimulated with Bic/4-AP (5 min) in the presence or absence of oligomycin and 2-deoxy-D-glucose (Oligo/2-DG, 5-min pre-treatment 1 μM/50 mM). Cell extracts were then probed on phosphoprotein arrays ((A)–(D), upper boxes show phosphorylated ERK1/2 [$Thr^{202}/Tyr^{204}$, $Thr^{185}/Tyr^{187}$] and lower boxes show phosphorylated AMPK [$Thr^{172}$]).

(E) Quantification of the kinase array represented as a heatmap; results are expressed as percentage of the control (Ctrl).

(F) Intracellular ATP quantifications following 5-min Oligo/2-DG treatment (n = 3).

(G) Western blot (WB) analysis of phosphorylated ACC and AMPK and total ACC, AMPK, and actin in lysates obtained from 15 DIV neurons stimulated with Bic/4-AP for the indicated times. WB is representative of at least 4 independent experiments.

(H and I) WB quantifications showing the ratios of phosphorylated AMPK/total AMPK (pAMPK/AMPK) (H) and phosphorylated ACC/total ACC (pACC/ACC) (I) following Bic/4-AP stimulation (n = 4).

Results show means ± SD. Student's t test (F) and one-way ANOVA with Bonferonni post-hoc test (H–I) were used for evaluation of statistical significance. *p < 0.05, **p < 0.01, ***p < 0.001. See also Figures S1 and S2.

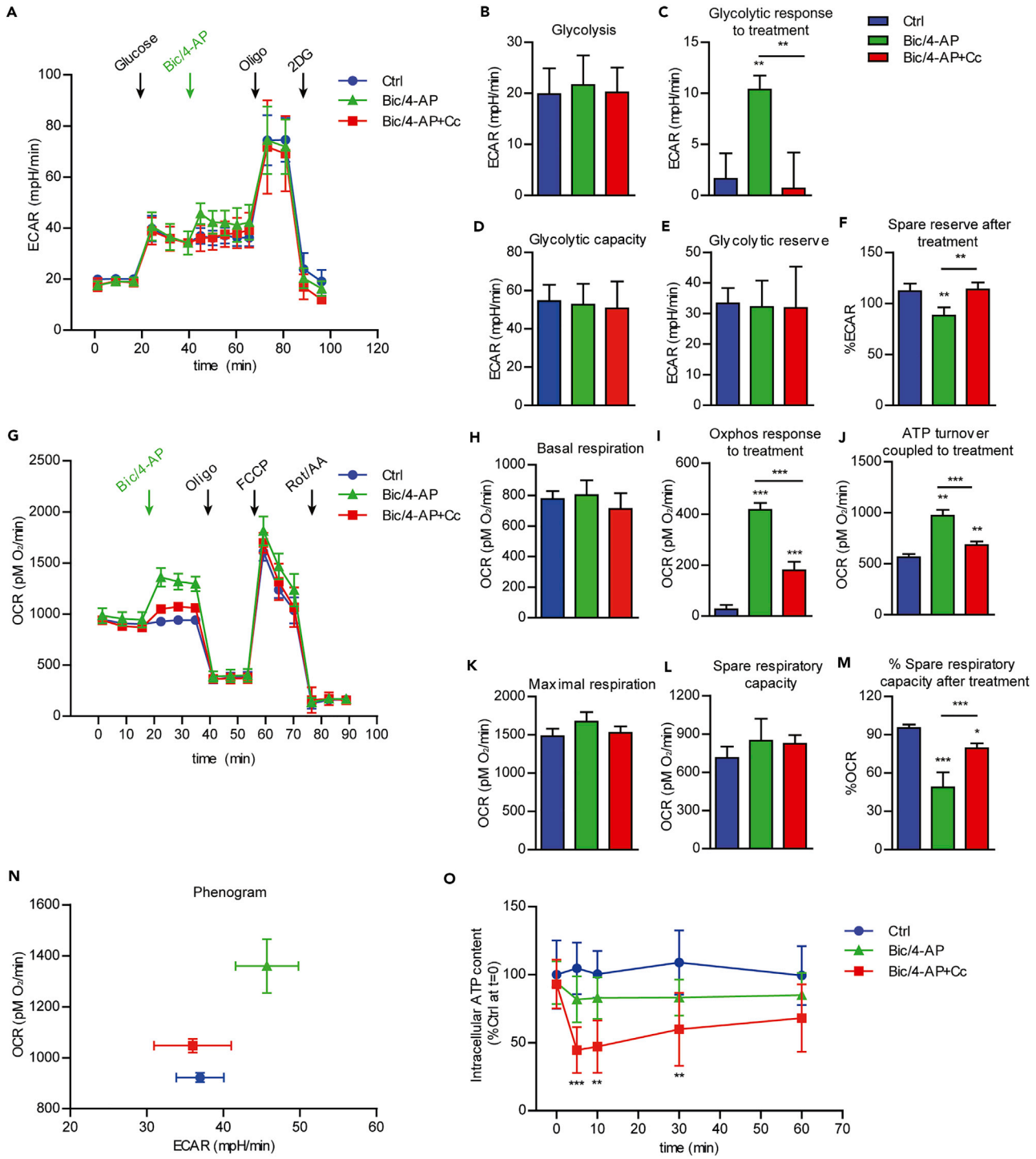


**Figure 2. AMPK Maintains Energy Levels by Up-regulating Glycolysis and Mitochondrial Respiration during Synaptic Activity**

(A–M) Extracellular acidification rate (ECAR, A) and oxygen consumption rate (OCR, G) measured using the Seahorse XFe24 technology after Bic/4-AP stimulation (green arrows) in the presence or absence of the AMPK inhibitor compound C (Cc, 10 μM). (A) ECAR profile is monitored under basal conditions and upon the sequential injection of saturating concentration of glucose, followed by Bic/4-AP, or assay medium in control (Ctrl) group, oligomycin (Oligo), and 2-deoxy-D-glucose (2-DG) as indicated by arrows. (G) OCR profile monitored under basal condition and following the sequential injection of assay medium, in Ctrl group, or Bic/4-AP, in the stimulated groups, Oligo, carbonyl cyanide-4-(trifluoromethoxy)phenylhydrazone (FCCP), and rotenone and antimycin A (Rot/AA) as indicated by arrows. ECAR and OCR are indicators of glycolysis and mitochondrial respiration, respectively. (B) Basal glycolysis, (C) glycolytic response to treatment, (D) glycolytic capacity, (E) spare glycolytic reserve expressed as mpH/min, (F) spare glycolytic reserve after treatment

**Figure 2. *Continued***

expressed as percentage of baseline, (H) basal respiration, (I) oxphos response to treatment, (J) ATP turnover coupled to treatment, (K) maximal respiration, (L) spare respiratory capacity expressed as pM $O_2$/min, and (M) spare respiratory capacity after treatment expressed as percentage of baseline were calculated as described in the Methods section; n = 4–5.

(N) Phenogram obtained by plotting the values obtained from the study of glycolysis (A) and mitochondrial respiration (G) following Bic/4-AP stimulation.

(O) Intracellular ATP levels in neurons stimulated with Bic/4-AP for the indicated times in the presence or absence of Cc (n = 3–4). Values are expressed as percentage of ATP in the Ctrl at time 0.

Results show mean ± SD. One-way ANOVA (B–F and H–M) and two-way ANOVA (O) followed by Bonferroni's post-hoc test were used for the evaluation of statistical significance. *$p < 0.05$, **$p < 0.01$, ***$p < 0.001$. See also Figures S3–S5 and S7.

## AMPK Activation Is Necessary to Induce Neuronal Metabolic Plasticity in Response to Synaptic Activation

To test whether AMPK was involved in the maintenance of energy levels during SA, we assessed metabolic fluxes in differentiated live neurons using the extracellular flux analyzer Seahorse XFe24 (Marinangeli et al., 2018). Glycolytic flux was determined by measuring the extracellular acidification rate (ECAR) due to $H^+$ release in combination with lactate, and mitochondrial respiration was determined by measuring the oxygen consumption rate (OCR). Following Bic/4-AP stimulation, ECAR and OCR were increased, showing that both glycolysis and mitochondrial respiration were enhanced to maintain energy levels following SA (Figures 2A and 2G, green arrows, and Figures 2C and 2I). Several metabolic parameters were determined using calculations described in the Methods section. Interestingly, Bic/4-AP stimulation did not change the overall glycolytic reserve (Figure 2E), maximal respiration (Figure 2K), or spare respiratory capacity (Figure 2L). However, in the presence of Bic/4-AP stimulation, the cells engage a larger fraction of the existing glycolytic reserve (Figure 2F) and spare respiratory capacity (Figure 2M) to increase energy production (Figure 2J). To determine the involvement of AMPK in this metabolic up-regulation induced following SA, neurons were pre-treated with the AMPK inhibitor compound C (Cc). Our results showed that AMPK inhibition prohibited the up-regulation of glycolysis and mitochondrial respiration that were induced by SA (Figures 2A–2M). Although AMPK inhibition in basal conditions (without SA induction) did not affect overall basal glycolysis or mitochondrial functions (Figure S3), it significantly reduced the use of the spare glycolytic reserve and spare respiratory capacity induced by SA (Figures 2F and 2M). Similar results were obtained using a kinase-dead dominant-negative construct of AMPK therefore excluding any potential off-target effect of Cc (Figures S4A and S4B). Finally, the phenogram analysis, which defines the overall cellular metabolic state of the cells, demonstrated that SA induced by Bic/4-AP led to a shift toward a metabolic state of the neurons (Figure 2N) that we will refer to as their metabolic plasticity. AMPK inhibition using Cc almost completely abolished this shift (Figure 2N), thereby suggesting that AMPK activity is necessary to maintain energy levels during SA. To confirm this, intracellular ATP levels were quantified in neurons at different time points following SA in the presence or absence of Cc. In control and SA conditions ATP levels remained constant, whereas AMPK repression led to a significant rapid drop in ATP levels in conditions of SA (Figure 2O). These results showed that AMPK activity following SA is essential to maintain neuronal energy levels.

## AMPK Up-regulates Mitochondrial Respiration in Response to Synaptic Activation

Glycolysis and mitochondrial respiration are tightly coupled together. Given that neurons are mainly oxidative cells, we asked whether the increase in mitochondrial respiration induced by SA was dependent on glycolysis up-regulation or whether AMPK could have a more direct impact on mitochondria. To assess the latter, we investigated its involvement in the oxidation of mitochondrial substrates that do not require prior glycolysis. As neurons were reported to use lactate as an alternative substrate to glucose in the context of the astrocyte-neuron lactate shuttle, we substituted glucose with lactate in the Seahorse XFe24 experiments. In these conditions, SA up-regulated mitochondrial respiration (Figures S5A–S5F), as it was previously observed with glucose. This metabolic response to SA was inhibited by the presence of Cc, showing that AMPK is also involved in the regulation of lactate utilization following SA. Importantly, these results support a more direct role of AMPK in mitochondrial function. Given that neurons were also reported to use glutamine for energy (Divakaruni et al., 2017), we repeated these experiments with a media devoid of glucose. Results showed that following SA, neurons did not use the glutamine present in the culture media to increase their energy production (Figures S5G–S5L). To go further, we performed metabolomics to determine the fluxes throughout the central carbon metabolism using $^{13}C$ stable-isotope tracing. For this, neurons were cultured in the presence of uniformly $^{13}C$-labeled glucose, and fractional contribution was quantified using mass spectrometry (isotopologs were designated as m0, m1, m2, m3, …). An increase in labeled lactate confirmed the increased glycolytic flow under SA conditions that was prohibited

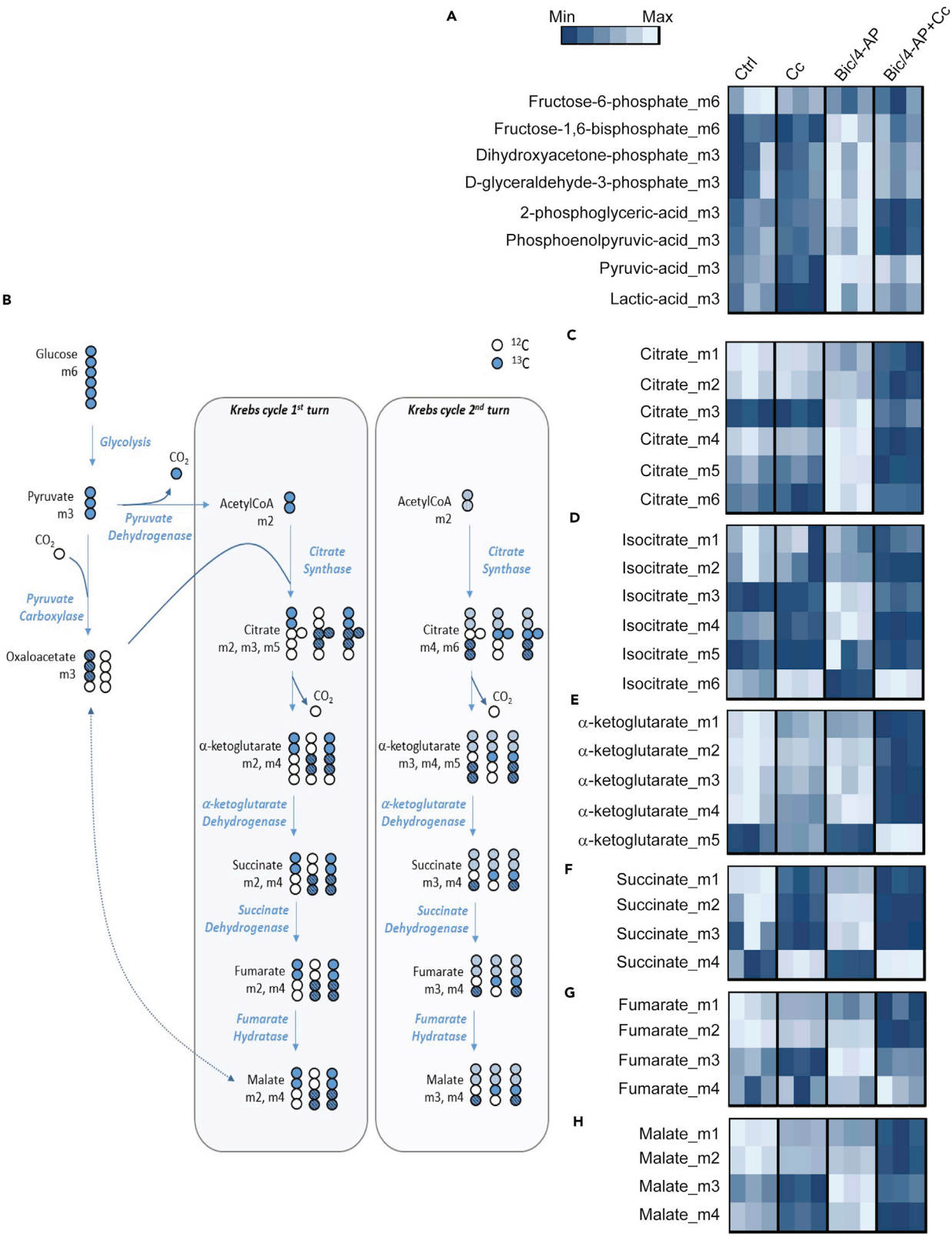
A
Min
Max
Ctrl
Cc
Bic/4-AP
Bic/4-AP+Cc
Fructose-6-phosphate_m6
Fructose-1,6-bisphosphate_m6
Dihydroxyacetone-phosphate_m3
D-glyceraldehyde-3-phosphate_m3
2-phosphoglyceric-acid_m3
Phosphoenolpyruvic-acid_m3
Pyruvic-acid_m3
Lactic-acid_m3
B
12C
13C
Glucose m6
Glycolysis
CO2
Pyruvate m3
Pyruvate Dehydrogenase
CO2
Pyruvate Carboxylase
Oxaloacetate m3
Krebs cycle 1st turn
Krebs cycle 2nd turn
AcetylCoA m2
Citrate Synthase
Citrate m2, m3, m5
CO2
α-ketoglutarate m2, m4
α-ketoglutarate Dehydrogenase
Succinate m2, m4
Succinate Dehydrogenase
Fumarate m2, m4
Fumarate Hydratase
Malate m2, m4
AcetylCoA m2
Citrate Synthase
Citrate m4, m6
CO2
α-ketoglutarate m3, m4, m5
α-ketoglutarate Dehydrogenase
Succinate m3, m4
Succinate Dehydrogenase
Fumarate m3, m4
Fumarate Hydratase
Malate m3, m4
C
Citrate_m1
Citrate_m2
Citrate_m3
Citrate_m4
Citrate_m5
Citrate_m6
D
Isocitrate_m1
Isocitrate_m2
Isocitrate_m3
Isocitrate_m4
Isocitrate_m5
Isocitrate_m6
E
α-ketoglutarate_m1
α-ketoglutarate_m2
α-ketoglutarate_m3
α-ketoglutarate_m4
α-ketoglutarate_m5
F
Succinate_m1
Succinate_m2
Succinate_m3
Succinate_m4
G
Fumarate_m1
Fumarate_m2
Fumarate_m3
Fumarate_m4
H
Malate_m1
Malate_m2
Malate_m3
Malate_m4

**Figure 3. AMPK Up-regulates Mitochondrial Metabolism upon Synaptic Activation**

Measurement of $^{13}$C-glucose-derived metabolites, calculated as percentage of the total metabolite pool following liquid chromatography-mass spectrometry analysis of primary neurons after 30 min in culture with $^{13}$C-glucose-supplemented media with or without Bic/4-AP stimulation.

(A) Metabolic profile of glycolysis intermediates.

(B) Schematic representation of the labeling patterns of metabolic intermediates starting from uniformly labeled glucose. The letter "m" indicates the number of carbon atoms labeled with $^{13}$C. The blue filled circles represent $^{13}$C atoms derived from pyruvate dehydrogenase activity, whereas the dashed circles represent $^{13}$C atoms derived from the pyruvate carboxylase activity.

(C–H) Isotopolog quantification of the Krebs cycle intermediates citrate (C), isocitrate (D), α-ketoglutarate (E), succinate (F), fumarate (G), and malate (H). Metabolic profiles are expressed as heatmaps. n = 3.

See also Figure S5.

by Cc (Figure 3A). Furthermore, analysis of the isotopolog profiles of the tricarboxylic acid cycle (TCA) metabolites demonstrated significant changes (Figures 3B–3H). Of particular interest is the significant increase in the levels of m3 isotopomers in SA from citrate, succinate, fumarate, and malate, suggesting that SA induced a shift toward pyruvate carboxylation (Buescher et al., 2015). Higher abundances of m4, m5, and m6 isotopologs from citrate were observed following Bic/4-AP stimulation (Figure 3C). These isotopomers require the combined action of pyruvate dehydrogenase (PDH), pyruvate carboxylase (PC), and multiple turns of the Kerbs cycle, as explained in Figure 3B. These results suggest that Bic/4-AP stimulation induced a shift toward anaplerotic pyruvate carboxylation that was not observed when AMPK activity was repressed. Altogether, these data support the notion that AMPK activity is needed to induce the metabolic "reprogramming" that occurs following SA.

## Neuronal Metabolic Plasticity Induced by AMPK Is Crucial for Immediate-Early Genes Expression, Synaptic Plasticity, and Long-Term Memory Formation

We next sought to determine the importance of this metabolic plasticity regulated by AMPK for neuronal functions. SA, when sustained, leads to the expression of immediate-early genes (IEGs) that include Arc, cFos, and Egrl. These genes are known to modulate the neuronal plasticity underlying learning and memory. In our model of SA, we observed the expression of these IEGs starting 1 hr after Bic/4-AP treatment (Figure 4A). This induction of IEG expression was inhibited when the energetic status was disrupted by either the inhibition of glycolysis with the glyceraldehyde-3-phosphate dehydrogenase inhibitor iodoacetate or 2-DG or the interruption of mitochondrial respiration using oligomycin and the inhibitors of complexes I and III rotenone and antimycin A, respectively (Figure 4B). These results demonstrated that the maintenance of energy levels is crucial for the expression of IEGs. In addition, AMPK inhibition also led to a significant reduction of IEG expression following SA (Figures 4C and S4C), showing that AMPK-mediated metabolic plasticity is necessary for the expression of IEGs following SA.

To examine the impact of AMPK inhibition on synaptic plasticity under more physiological conditions, we took advantage of *ex vivo* hippocampal slices. Thus, we investigated a putative role of AMPK in long-term potentiation (LTP) in the CA1 region of the hippocampus, a well-established model of learning and memory at the cellular level. As depicted in Figure 4D, triple application of an electrical theta burst stimulation protocol resulted in robust LTP in control (vehicle) with initial values of 213.3 ± 5.3% (n = 7), which were retained at about this level until 4 hr after induction (197.5 ± 15.1%). This robust type of LTP is protein synthesis dependent and therefore a relevant model for the formation of long-term memory (Ahmed and Balschun, unpublished data). Application of 10 μM Cc, in contrast, caused a severe impairment of LTP with a significantly lower initial magnitude of 146.2 ± 9.4% ($p = 0.0001$ Welch test) and a decremental potentiation that returned to baseline values after about 80 min (Wilcoxon test). Overall, this resulted in a highly significant difference in LTP in control mice ($F_{1,13} = 120.105$; $p < 0.001$, repeated measures (RM)-ANOVA) underlining an essential function of AMPK in long-term synaptic plasticity. Furthermore, quantification of the LTP defect, in percentage, of control for the average of first 30 min used as a measure of induction (vehicle LTP: 200% ± 7%, n = 11; Cc LTP: 126% ± 6%, n = 8; RM-ANOVA [$F_{1,17}$] = 25.58, $p < 0.0001$) and for the average of 210–240 min used as a measure of late maintenance (vehicle LTP: 159% ± 9%, n = 11; Cc LTP: 77% ± 11%, n = 8; RM-ANOVA [$F_{1,17}$] = 25.58 $p < 0.0001$) demonstrated that Cc reduced both the induction and the late maintenance phases.

Finally, to evaluate the importance of AMPK-mediated metabolic plasticity *in vivo*, we tested whether AMPK activation is involved in long-term memory retention. To this end, Cc was bilaterally injected in the hippocampus of awake wild-type mice 20 min before inhibitory avoidance (IA) training, a task that depends on the proper functioning of the hippocampus (Izquierdo et al., 2016; Whitlock et al., 2006) (Figures

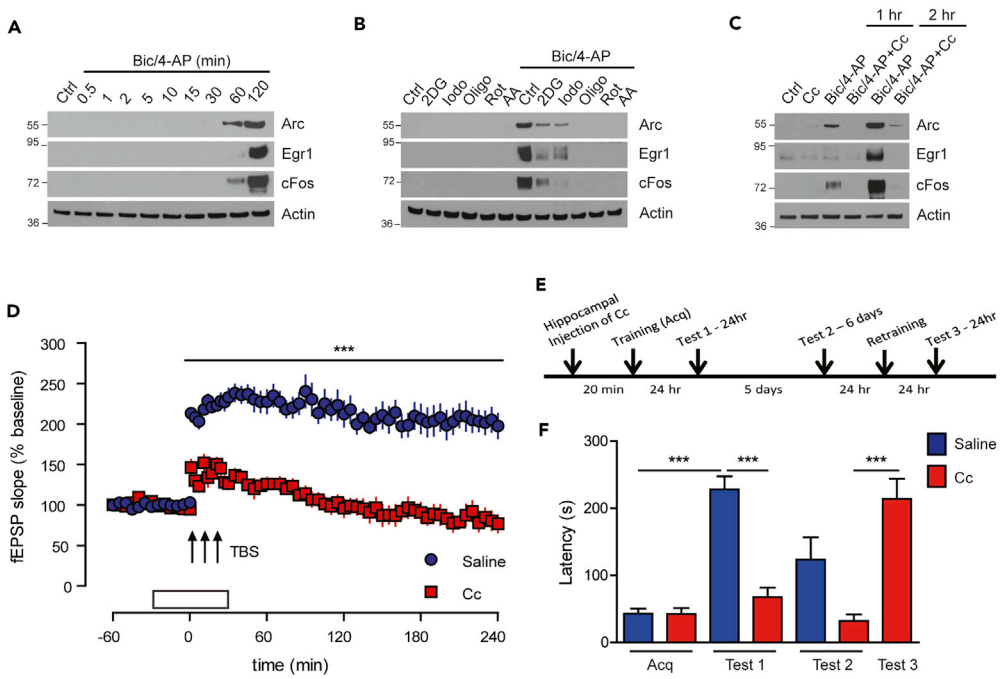


**Figure 4. AMPK Activation Following Synaptic Activity Is Necessary for IEG Expression, Synaptic Plasticity, and Long-Term Memory Formation**

(A) Western blot (WB) analysis of the IEGs Arc, Egrl, and cFos expression following Bic/4-AP stimulation for the indicated times in differentiated primary neurons at 15 DIV (days *in vitro*). WB is representative of at least 5 independent experiments.

(B) WB analysis of the IEGs Arc, Egrl, and cFos expression following 2 hr Bic/4-AP stimulation in the presence or absence of glycolysis inhibitors (2-DG 50 mM, Iodo 100 μM pre-treatment of 5 min) or mitochondrial respiration inhibitors (Oligo 1 μM, rotenone [Rot] 1 μM, antimycin A [AA] 1 μM pre-treatment of 5 min) in differentiated primary neurons at 15 DIV. WB is representative of at least 4 independent experiments.

(C) WB analysis of the IEGs Arc, Egrl, and cFos expression following 2 hr Bic/4-AP stimulation in the presence or absence of Cc (20 min pre-treatment, 10 μM). WB is representative of at least 4 independent experiments.

(D) Recording of LTP in the CA1 region of the hippocampus *ex vivo*. Triple application of an electrical theta burst stimulation protocol induced robust LTP in controls. However, in slices treated with 10 μM Cc, the same stimulation generated only an impaired, decremental potentiation, returning to baseline values after about 80 min (Wilcoxon test). This resulted in a highly significant difference ($F_{1,13}$ = 120.105; $p < 0.001$, RM-ANOVA). Data are presented as mean ± SEM, where n refers to the number of animals tested.

(E) Schematic representation of the IA protocol timeline.

(F) Hippocampal injections of Cc 20 min before the IA training (Acq) disrupted long-term memory at 24 hr (Test 1). The disruption persisted 6 days after training (Test 2). Cc-injected mice had normal retention after retraining (Test 3). n = 10, results show mean ± SEM.

One-way ANOVA followed by Bonferroni's post-hoc test was used for evaluation of statistical significance. ***$p < 0.001$. See also Figure S4.

4E and 4F). Cc injection did not affect IA acquisition, as the mean latencies to enter the shock compartment during training (Acq) were similar in both groups. However, Cc significantly blocked long-term memory tested at 24 hr (Test 1). Retesting 6 days after acquisition (Test 2) showed that the memory loss persisted. Retraining of the Cc injected group resulted in normal memory retention 24 hr later (Test 3), indicating that the hippocampus was functionally intact. Altogether, these results show that AMPK is involved in long-term memory formation and provided proof of concept that AMPK plays an essential role in cognitive processes.

## AMPK Deregulation Impairs the Neuronal Metabolic Plasticity Induced by Synaptic Activation

Last, we asked whether AMPK deregulation as it is observed in AD could impair AMPK-mediated metabolic plasticity induced by SA. Since AMPK is over-activated in neurons of patients with AD when compared with

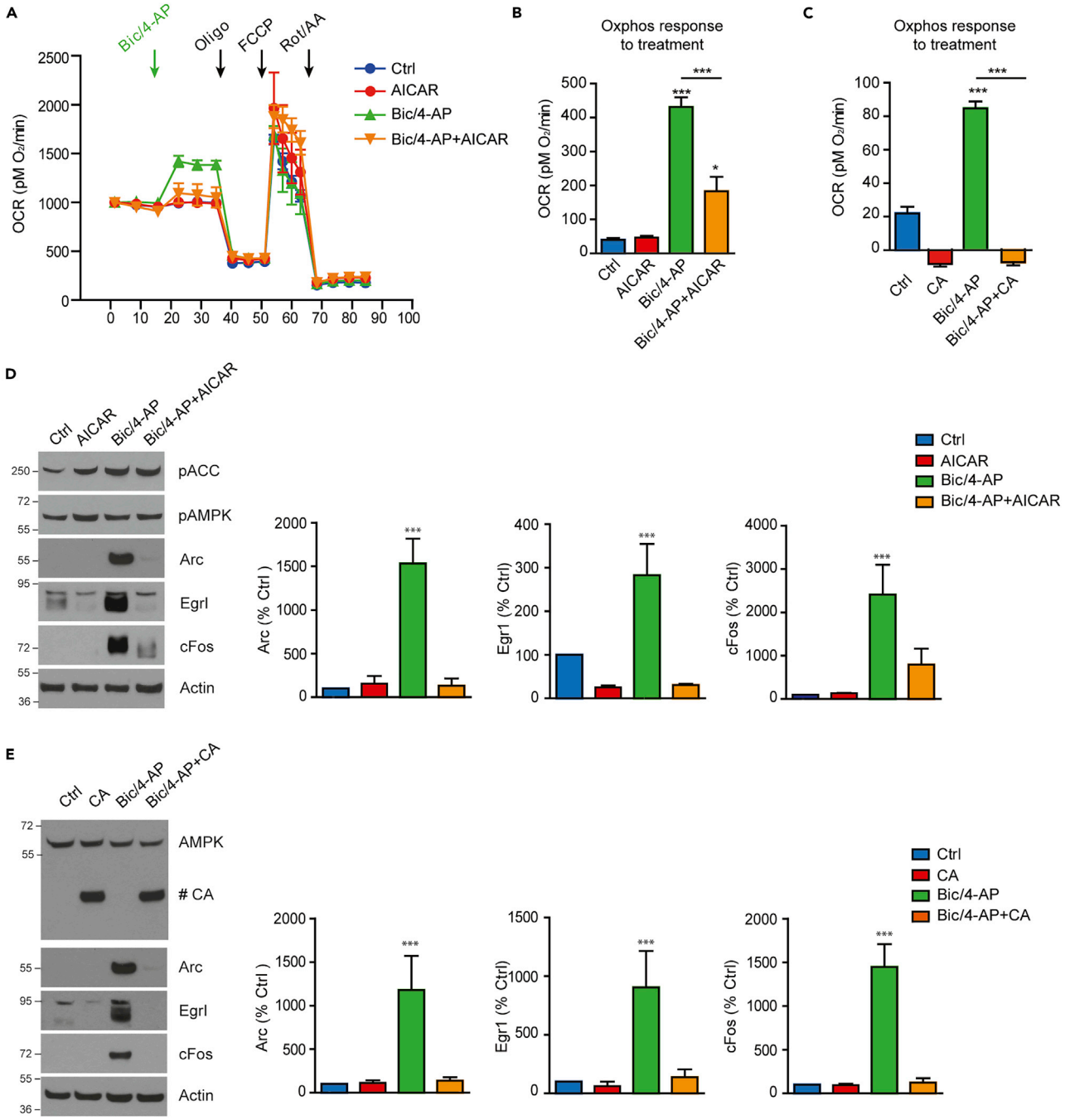


**Figure 5. AMPK Pre-activation Prevents Neuronal Metabolic Response to SA**

(A) Mitochondrial respiration profile in primary neurons evaluated using the Seahorse XFe24 technology to investigate the impact of long-lasting (24 hr) AMPK activation induced by AICAR in response to Bic/4-AP. Mitochondrial respiration profile, expressed as oxygen consumption rate (OCR), is monitored upon the injection of assay medium, in control group (Ctrl) and in cells treated with AICAR (AICAR), or upon the injection of Bic/4-AP in the absence (Bic/4-AP) or presence of AICAR (Bic/4-AP + AICAR), followed by injection of Oligo, carbonyl cyanide-4-(trifluoromethoxy)phenylhydrazone (FCCP), and rotenone and antimycin A [Rot/AA] as indicated by the arrows. Results are representative of 3 independent experiments.

(B) OCR response to Bic/4-AP stimulation expressed as $pMO_2$/min (n = 3).

(C) OCR response to Bic/4-AP stimulation expressed as $pMO_2$/min in primary neurons over-expressing a constitutively active (CA) form of AMPK (n = 3).

(D) Immunoblotting with phosphorylated ACC (pACC), phosphorylated AMPK (pAMPK), Arc, Egrl, cFos, and actin in lysates obtained from 15 days *in vitro* (DIV) neurons stimulated with Bic/4-AP for 2 hr after pre-treatment with AICAR (24 hr, 1 mM). Results are representative of at least 5 independent experiments. Quantification of western blot (WB) showing the expression of the IEGs Arc, Egrl, and cFos (n = 5).

**Figure 5. *Continued***

(E) Immunoblotting with total AMPK (# CA labels the over-expressed CA-AMPK construct), Arc, Egrl, cFos, and actin in lysates obtained from 15 DIV neurons stimulated with Bic/4-AP for 2 hr, 4 days after injection with CA-AMPK. Results are representative of at least 3 experiments. Quantification of WB showing the expression of the IEGs Arc, Egrl, and cFos (n = 3).

Results show mean ± SD. One-way ANOVA followed by Bonferroni's post-hoc test was used for evaluation of statistical significance. *$p < 0.05$, ***$p < 0.001$. See also Figures S6 and S7.

control patients (Vingtdeux et al., 2011), we mimicked this condition by treating primary neurons with AICAR, an AMPK agonist, 24 hr before inducing SA (referred to as pre-activation hereafter). AMPK pre-activation with AICAR did not modify the metabolic profile of neurons, whereas it greatly impaired the ability of neurons to up-regulate mitochondrial respiration in response to SA (Figures 5A and 5B). Similar results were obtained after over-expression of a constitutively active mutant of AMPK (CA-AMPK) in neurons (Figure 5C), further supporting the inhibitory effect of AMPK pre-activation on the metabolic response to SA. We then assessed the effect of AMPK pre-activation on neuronal ATP content during SA (Figure S6). Our results showed that, when compared with unstimulated cells, ATP content, both in control and AICAR pre-treated groups remained constant during SA. These results suggest that AMPK pre-activation might have produced metabolic alterations that prevented SA from occurring in a different way than the acute inhibition observed with Cc. In this context, the pre-activation of AMPK either using AICAR or CA-AMPK also prevented the SA-induced expression of IEGs (Figures 5D and 5E). Altogether, our results show that a tight regulation of AMPK is important for the physiological metabolic response of neurons to SA and for the triggering of processes leading to neuronal plasticity.

## DISCUSSION

Neurons have high energy demands that are met through the oxidation of glucose via glycolysis and mitochondrial respiration. Neuronal activity is a process known to require and thus stimulate ATP production (Rangaraju et al., 2014); however, the molecular mechanisms involved in this regulation remain poorly understood. Here, we demonstrated that the AMPK-mediated signaling pathway plays a key role in this regulation. We found that AMPK is rapidly activated following SA to maintain energy levels via the up-regulation of glycolytic and mitochondrial use of glucose. Regulation of glucose uptake by AMPK in neurons has been previously described. AMPK was proposed to regulate glucose transporters GLUT3 and GLUT4 surface expression following glutamate excitation and action potential firing, respectively (Ashrafi et al., 2017; Weisova et al., 2009). It is possible that a mobilization of glucose transporters to the plasma membrane also occurs in our conditions, which could explain how AMPK regulates glycolysis. Our results, in addition to validate the increased glycolysis following SA, also demonstrate that mitochondrial respiration plays an important part in sustaining energy levels. Indeed, our data demonstrate that AMPK also acts on mitochondrial respiration independent of glycolysis. Actually, consistent with their high energy requirements, neurons sustain a high rate of oxidative metabolism (Boumezbeur et al., 2010). Bearing this in mind, the importance of mitochondria for cognitive functions has recently regained importance. In particular, a recent study has shown that cannabinoid receptors present on mitochondria (mtCB1) are responsible for amnesia induced by acute cannabinoid intoxication. In particular, activation of hippocampal mtCB1 receptors led to memory impairments due to decreased mitochondrial respiration (Hebert-Chatelain et al., 2016). Our study reinforces this link between mitochondrial activity and memory formation. Our results also raised the question of AMPK subcellular localization. Indeed, it could be speculated that a pool of AMPK might be present at or within the mitochondria to up-regulate mitochondrial respiration. Previous reports have also highlighted this possibility (Liang et al., 2015). In our context, further work will be required to determine whether PC or PDH could be direct AMPK substrates. In particular, PC catalyzes the conversion of pyruvate to oxaloacetate, named pyruvate carboxylation, within the mitochondria. Although this step, which leads to *de novo* synthesis of TCA cycle intermediates is crucial to replenish TCA cycle and supports the formation of transmitter glutamate, is widely described to occur in astrocytes, PC activity was also reported in neurons (for review see [Hassel and Brathe, 2000]). Another way to replenish TCA is via glutaminolysis. Although this possibility cannot be excluded, it seems not to be involved in our model given that the experiments performed without glucose did not show any response to SA, although glutamine was present in cell culture media. Another interesting possibility is the regulation by AMPK of the AKAP1 (A kinase anchor protein 1) protein, which was identified in muscle by a global phosphoproteomic approach (Hoffman et al., 2015). This direct phosphorylation of AKAP1 by AMPK was reported to regulate mitochondrial respiration (Hoffman et al., 2015). Although we assessed only the immediate metabolic response of neurons to synaptic activity, it will also be interesting to determine whether AMPK could be involved in gene expression changes that

promote the neuronal Warburg effect in response to prolonged Bic/4-AP stimulation (Bas-Orth et al., 2017).

Our results are also particularly important in the context of neurodegenerative disorders in which energy metabolism is strongly impaired and AMPK is over-activated (Jiang et al., 2013; Ju et al., 2011; Vingtdeux et al., 2011). In conditions of over-activation, AMPK is unlikely to respond properly to SA, perhaps as a way to preserve energy levels. As a consequence, we propose that AMPK might act as a metabolic switch that determines whether SA may or may not occur according to the currently available energy levels (and hence metabolic substrate) in its vicinity. It is also possible that AMPK over-activation could indirectly impair the metabolic plasticity response to SA. Under these conditions, the identification of AMPK targets as well as the consequences of AMPK over-activation on synaptic integrity will be of interest. Supporting this hypothesis, previous reports have determined that AMPK activation by pharmacological drugs led to impairments in synaptic plasticity (Potter et al., 2010) and memory formation (Dash et al., 2006). In addition, in the context of AD, AMPK was proposed to be a key player in the reduction of number of dendritic spine (Mairet-Coello et al., 2013) and in the LTP impairments induced by Aβ oligomers (Ma et al., 2014). These reports show that up-regulation of AMPK activity has the same negative outcome on synaptic plasticity and memory formation as AMPK inhibition.

Altogether, our data suggest that AMPK activity has to be fine-tuned extremely well since any hypo- or hyperactivation will have detrimental consequences on synaptic plasticity and hence memory formation.

In summary, our results demonstrate that AMPK plays a critical role during glutamatergic SA. In particular, we show that AMPK activity is crucial to maintain neuronal energy levels and hence is involved in memory formation processes. Our study establishes AMPK as an important link between memory formation and energy metabolism and suggests that it could act as a metabolic checkpoint by sensing the availability of energy substrates. These findings might also be of value in the context of diabetes and obesity, conditions that are associated with cognitive (Dye et al., 2017; McCrimmon et al., 2012) and central metabolism (Hwang et al., 2017) impairments in humans.

### Limitations of Study

Our data also demonstrate that the energetic metabolic up-regulation mediated by AMPK is crucial for the expression of IEGs, synaptic plasticity, and long-term memory formation. In line with these results, AMPK was reported to be activated and necessary for LTP induced *in vivo* by high-frequency stimulation (Yu et al., 2016). However, our *in vivo* data were obtained using a pharmacological approach to inhibit AMPK; therefore for a more thorough understanding of these processes, the generation of conditional AMPK knockout mouse models will be necessary to disentangle the importance of neuronal AMPK in particular types and phases of memory.

## METHODS

All methods can be found in the accompanying Transparent Methods supplemental file.

## SUPPLEMENTAL INFORMATION

Supplemental Information includes Transparent Methods and seven figures and can be found with this article online at https://doi.org/10.1016/j.isci.2018.10.006.

## ACKNOWLEDGMENTS

We thank the animal core facility (animal facilities of Université de Lille-Inserm) of "Plateformes en Biologie Santé de Lille" as well as C. Degraeve, M. Besegher-Dumoulin, J. Devassine, R. Dehaynin, and D. Taillieu for animal care. The authors thank the behavioral exploration platform for rodent (Federation of Neurosciences, Univ. Lille, France). pAMPK alpha2 WT and pAMPK alpha2 K45R were a gift from Morris Birnbaum (Addgene plasmids # 15991 and 15992).

This work was supported by the French Fondation pour la cooperation Scientifique—Plan Alzheimer 2008-2012 (Senior Innovative Grant 2013) to V.V., by the Fondation Vaincre Alzheimer (n°FR-16071p) to V.V., and in part by the Labex DISTALZ (Development of Innovative Strategies for a Transdisciplinary Approach to Alzheimer's disease) to L.B.; by INSERM, UNIVERSITE DE LILLE II, Ligue Contre le Cancer (Comité du

Nord, Comité de l'Aisne) to P.M. and J.K.; and a special financial support from the Association pour l'Etude des Anomalies Congénitales Neurodev of Pr. B. Poupard to P.M. T.A. and D.B. are supported by the Fonds voor Wetenschappelijk Onderzoek (FWO) Flanderen, project G0D7614N. M.D. holds a doctoral scholarship from Lille 2 University.

## AUTHOR CONTRIBUTIONS

Conceptualization, J.K. and V.V.; Methodology, C.M., T.A., C.L., B.G., D.B., J.K., and V.V.; Investigation, C.M., S.D., T.A., R.C., M.D., B.G., J.K., and V.V.; Resources, S.B., S.C., M.C., P.M., and L.B.; Writing – Original Draft, C.M. and V.V.; Writing – Review & Editing, T.A., P.M., B.G., D.B., L.B., J.K., and V.V.; Supervision, J.K. and V.V.

## DECLARATION OF INTERESTS

The authors declare that they have no conflict of interest.

Received: June 4, 2018
Revised: September 1, 2018
Accepted: October 8, 2018
Published: November 30, 2018

## REFERENCES

Ashrafi, G., Wu, Z., Farrell, R.J., and Ryan, T.A. (2017). GLUT4 mobilization supports energetic demands of active synapses. Neuron *93*, 606–615.e3.

Attwell, D., and Laughlin, S.B. (2001). An energy budget for signaling in the grey matter of the brain. J. Cereb. Blood Flow Metab. *21*, 1133–1145.

Bas-Orth, C., Tan, Y.W., Lau, D., and Bading, H. (2017). Synaptic activity drives a genomic program that promotes a neuronal Warburg effect. J. Biol. Chem. *292*, 5183–5194.

Boumezbeur, F., Mason, G.F., de Graaf, R.A., Behar, K.L., Cline, G.W., Shulman, G.I., Rothman, D.L., and Petersen, K.F. (2010). Altered brain mitochondrial metabolism in healthy aging as assessed by in vivo magnetic resonance spectroscopy. J. Cereb. Blood Flow Metab. *30*, 211–221.

Buescher, J.M., Antoniewicz, M.R., Boros, L.G., Burgess, S.C., Brunengraber, H., Clish, C.B., DeBerardinis, R.J., Feron, O., Frezza, C., Ghesquiere, B., et al. (2015). A roadmap for interpreting (13)C metabolite labeling patterns from cells. Curr. Opin. Biotechnol. *34*, 189–201.

Caminiti, S.P., Ballarini, T., Sala, A., Cerami, C., Presotto, L., Santangelo, R., Fallanca, F., Vanoli, E.G., Gianolli, L., Iannaccone, S., et al. (2018). FDG-PET and CSF biomarker accuracy in prediction of conversion to different dementias in a large multicentre MCI cohort. Neuroimage Clin. *18*, 167–177.

Dash, P.K., Orsi, S.A., and Moore, A.N. (2006). Spatial memory formation and memory-enhancing effect of glucose involves activation of the tuberous sclerosis complex-mammalian target of rapamycin pathway. J. Neurosci. *26*, 8048–8056.

Divakaruni, A.S., Wallace, M., Buren, C., Martyniuk, K., Andreyev, A.Y., Li, E., Fields, J.A., Cordes, T., Reynolds, I.J., Bloodgood, B.L., et al. (2017). Inhibition of the mitochondrial pyruvate carrier protects from excitotoxic neuronal death. J. Cell Biol. *216*, 1091–1105.

Domise, M., and Vingtdeux, V. (2016). AMPK in neurodegenerative diseases. EXS *107*, 153–177.

Dye, L., Boyle, N.B., Champ, C., and Lawton, C. (2017). The relationship between obesity and cognitive health and decline. Proc. Nutr. Soc. *76*, 443–454.

Ferreira, I.L., Resende, R., Ferreiro, E., Rego, A.C., and Pereira, C.F. (2010). Multiple defects in energy metabolism in Alzheimer's disease. Curr. Drug Targets *11*, 1193–1206.

Gold, P.E. (1995). Role of glucose in regulating the brain and cognition. Am. J. Clin. Nutr. *61*, 987S–995S.

Hardingham, G.E., Fukunaga, Y., and Bading, H. (2002). Extrasynaptic NMDARs oppose synaptic NMDARs by triggering CREB shut-off and cell death pathways. Nat. Neurosci. *5*, 405–414.

Harris, J.J., Jolivet, R., and Attwell, D. (2012). Synaptic energy use and supply. Neuron *75*, 762–777.

Hassel, B., and Brathe, A. (2000). Neuronal pyruvate carboxylation supports formation of transmitter glutamate. J. Neurosci. *20*, 1342–1347.

Hawley, S.A., Boudeau, J., Reid, J.L., Mustard, K.J., Udd, L., Makela, T.P., Alessi, D.R., and Hardie, D.G. (2003). Complexes between the LKB1 tumor suppressor, STRAD alpha/beta and MO25 alpha/beta are upstream kinases in the AMP-activated protein kinase cascade. J. Biol. *2*, 28.

Hawley, S.A., Pan, D.A., Mustard, K.J., Ross, L., Bain, J., Edelman, A.M., Frenguelli, B.G., and Hardie, D.G. (2005). Calmodulin-dependent protein kinase kinase-beta is an alternative upstream kinase for AMP-activated protein kinase. Cell Metab. *2*, 9–19.

Hebert-Chatelain, E., Desprez, T., Serrat, R., Bellocchio, L., Soria-Gomez, E., Busquets-Garcia, A., Pagano Zottola, A.C., Delamarre, A., Cannich, A., Vincent, P., et al. (2016). A cannabinoid link between mitochondria and memory. Nature *539*, 555–559.

Hoey, S.E., Williams, R.J., and Perkinton, M.S. (2009). Synaptic NMDA receptor activation stimulates alpha-secretase amyloid precursor protein processing and inhibits amyloid-beta production. J. Neurosci. *29*, 4442–4460.

Hoffman, N.J., Parker, B.L., Chaudhuri, R., Fisher-Wellman, K.H., Kleinert, M., Humphrey, S.J., Yang, P., Holliday, M., Trefely, S., Fazakerley, D.J., et al. (2015). Global phosphoproteomic analysis of human skeletal muscle reveals a network of exercise-regulated kinases and AMPK substrates. Cell Metab. *22*, 922–935.

Hwang, J.J., Jiang, L., Hamza, M., Sanchez Rangel, E., Dai, F., Belfort-DeAguiar, R., Parikh, L., Koo, B.B., Rothman, D.L., Mason, G., et al. (2017). Blunted rise in brain glucose levels during hyperglycemia in adults with obesity and T2DM. JCI Insight *2*, e95913.

Izquierdo, I., Furini, C.R., and Myskiw, J.C. (2016). Fear memory. Physiol. Rev. *96*, 695–750.

Jiang, P., Gan, M., Ebrahim, A.S., Castanedes-Casey, M., Dickson, D.W., and Yen, S.H. (2013). Adenosine monophosphate-activated protein kinase overactivation leads to accumulation of alpha-synuclein oligomers and decrease of neurites. Neurobiol. Aging *34*, 1504–1515.

Ju, T.C., Chen, H.M., Lin, J.T., Chang, C.P., Chang, W.C., Kang, J.J., Sun, C.P., Tao, M.H., Tu, P.H., Chang, C., et al. (2011). Nuclear translocation of AMPK-alpha1 potentiates striatal neurodegeneration in Huntington's disease. J. Cell. Biol. *194*, 209–227.

Liang, J., Xu, Z.X., Ding, Z., Lu, Y., Yu, Q., Werle, K.D., Zhou, G., Park, Y.Y., Peng, G., Gambello, M.J., et al. (2015). Myristoylation confers

noncanonical AMPK functions in autophagy selectivity and mitochondrial surveillance. Nat. Commun. *6*, 7926.

Lin, M.T., and Beal, M.F. (2006). Mitochondrial dysfunction and oxidative stress in neurodegenerative diseases. Nature *443*, 787–795.

Ma, T., Chen, Y., Vingtdeux, V., Zhao, H., Viollet, B., Marambaud, P., and Klann, E. (2014). Inhibition of AMP-activated protein kinase signaling alleviates impairments in hippocampal synaptic plasticity induced by amyloid beta. J. Neurosci. *34*, 12230–12238.

Mairet-Coello, G., Courchet, J., Pieraut, S., Courchet, V., Maximov, A., and Polleux, F. (2013). The CAMKK2-AMPK kinase pathway mediates the synaptotoxic effects of Abeta oligomers through Tau phosphorylation. Neuron *78*, 94–108.

Marinangeli, C., Kluza, J., Marchetti, P., Buee, L., and Vingtdeux, V. (2018). Study of AMPK-regulated metabolic fluxes in neurons using the seahorse XFe analyzer. Methods Mol. Biol. *1732*, 289–305.

McCrimmon, R.J., Ryan, C.M., and Frier, B.M. (2012). Diabetes and cognitive dysfunction. Lancet *379*, 2291–2299.

Mosconi, L. (2005). Brain glucose metabolism in the early and specific diagnosis of Alzheimer's disease. FDG-PET studies in MCI and AD. Eur. J. Nucl. Med. Mol. Imaging *32*, 486–510.

Potter, W.B., O'Riordan, K.J., Barnett, D., Osting, S.M., Wagoner, M., Burger, C., and Roopra, A. (2010). Metabolic regulation of neuronal plasticity by the energy sensor AMPK. PLoS One *5*, e8996.

Rangaraju, V., Calloway, N., and Ryan, T.A. (2014). Activity-driven local ATP synthesis is required for synaptic function. Cell *156*, 825–835.

Suzuki, A., Stern, S.A., Bozdagi, O., Huntley, G.W., Walker, R.H., Magistretti, P.J., and Alberini, C.M. (2011). Astrocyte-neuron lactate transport is required for long-term memory formation. Cell *144*, 810–823.

Vingtdeux, V., Davies, P., Dickson, D.W., and Marambaud, P. (2011). AMPK is abnormally activated in tangle- and pre-tangle-bearing neurons in Alzheimer's disease and other tauopathies. Acta Neuropathol. *121*, 337–349.

Weisova, P., Concannon, C.G., Devocelle, M., Prehn, J.H., and Ward, M.W. (2009). Regulation of glucose transporter 3 surface expression by the AMP-activated protein kinase mediates tolerance to glutamate excitation in neurons. J. Neurosci. *29*, 2997–3008.

Whitlock, J.R., Heynen, A.J., Shuler, M.G., and Bear, M.F. (2006). Learning induces long-term potentiation in the hippocampus. Science *313*, 1093–1097.

Woods, A., Johnstone, S.R., Dickerson, K., Leiper, F.C., Fryer, L.G., Neumann, D., Schlattner, U., Wallimann, T., Carlson, M., and Carling, D. (2003). LKB1 is the upstream kinase in the AMP-activated protein kinase cascade. Curr. Biol. *13*, 2004–2008.

Xiao, B., Heath, R., Saiu, P., Leiper, F.C., Leone, P., Jing, C., Walker, P.A., Haire, L., Eccleston, J.F., Davis, C.T., et al. (2007). Structural basis for AMP binding to mammalian AMP-activated protein kinase. Nature *449*, 496–500.

Yu, D.F., Shen, Z.C., Wu, P.F., Guan, X.L., Chen, T., Jin, Y., Hu, Z.L., Ni, L., Wang, F., Chen, J.G., et al. (2016). HFS-triggered AMPK activation phosphorylates GSK3β and induces E-LTP in rat hippocampus in vivo. CNS Neurosci. Ther. *22*, 525–531.

**ISCI, Volume *9***

## Supplemental Information

# AMP-Activated Protein Kinase Is Essential for the Maintenance of Energy Levels during Synaptic Activation

**Claudia Marinangeli, Sébastien Didier, Tariq Ahmed, Raphaelle Caillerez, Manon Domise, Charlotte Laloux, Séverine Bégard, Sébastien Carrier, Morvane Colin, Philippe Marchetti, Bart Ghesquière, Detlef Balschun, Luc Buée, Jérôme Kluza, and Valérie Vingtdeux**

**Supplemental Figures**

**Figure S1**

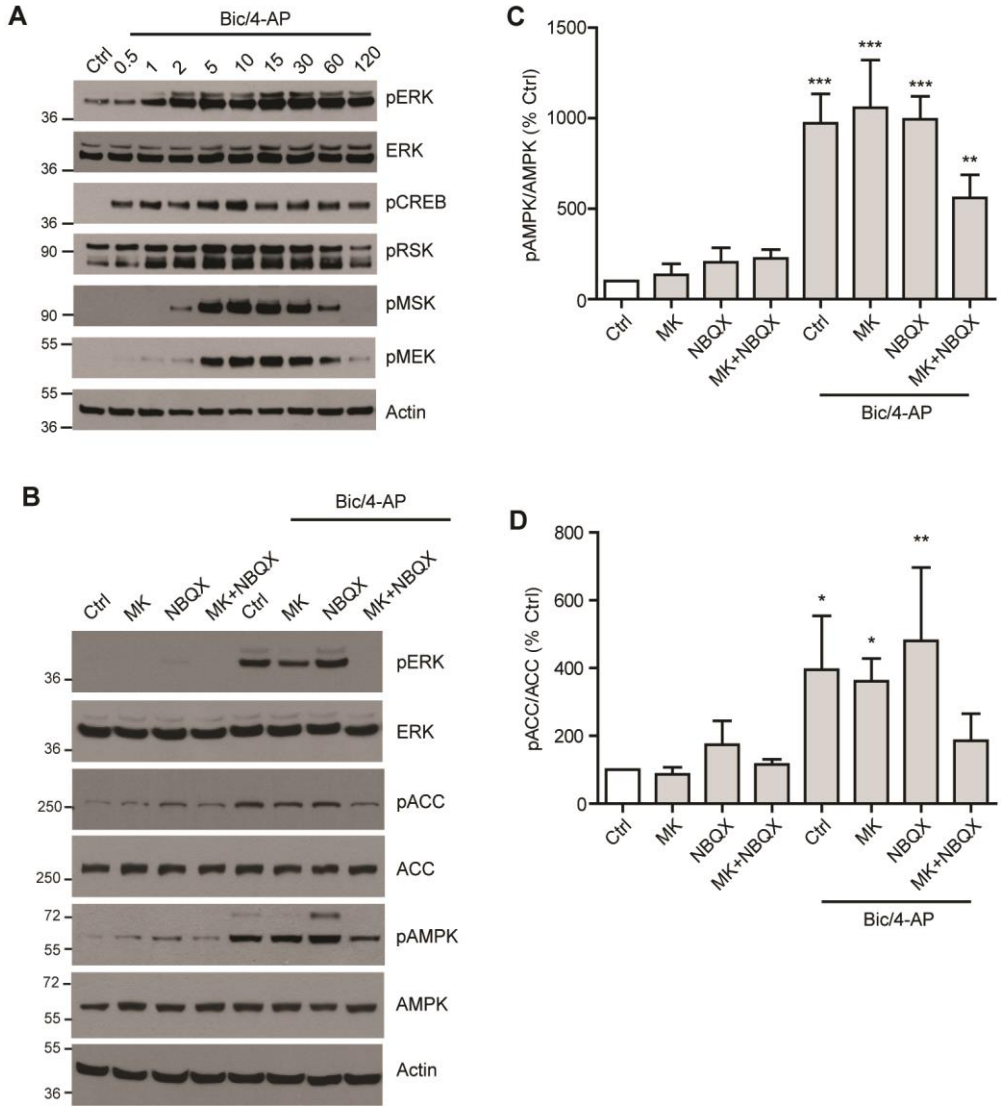


**Figure S1 - AMPK activation following SA is dependent on NMDA and AMPA receptors activation.** Related to Figure 1.

(**A**) Primary neurons were treated with Bic/4-AP for the indicated times and the activation of the MAPK pathway was monitored by immunoblotting with anti- phosphorylated ERK, CREB, RSK, MSK, MEK and total ERK and Actin antibodies. Results are representative of at least 3 experiments. (**B**) Primary neurons were pre-treated for 20 min with the NMDA receptors and AMPA receptors antagonists MK-801 (25 µM) and NBQX (20 µM), respectively. After pre-treatment, neurons were stimulated with Bic/4-AP for 10 min.

Activation of ERK and AMPK were monitored by immunoblotting with anti- phosphorylated ERK and total ERK and anti- phosphorylated AMPK and ACC, total AMPK, ACC, and Actin antibodies. Results are representative of at least 5 experiments. (**C-D**) Quantifications of WB as shown in B displaying the ratios phosphorylated AMPK/total AMPK (pAMPK/AMPK) and phosphorylated ACC/total ACC (pACC/ACC) expressed as percentage of control (n=3-5).

Results show mean ± SD. One-way ANOVA followed by Bonferroni's post-test was used for evaluation of statistical significance. * $p < 0.05$, ** $p < 0.01$, *** $p < 0.001$.

**Figure S2**

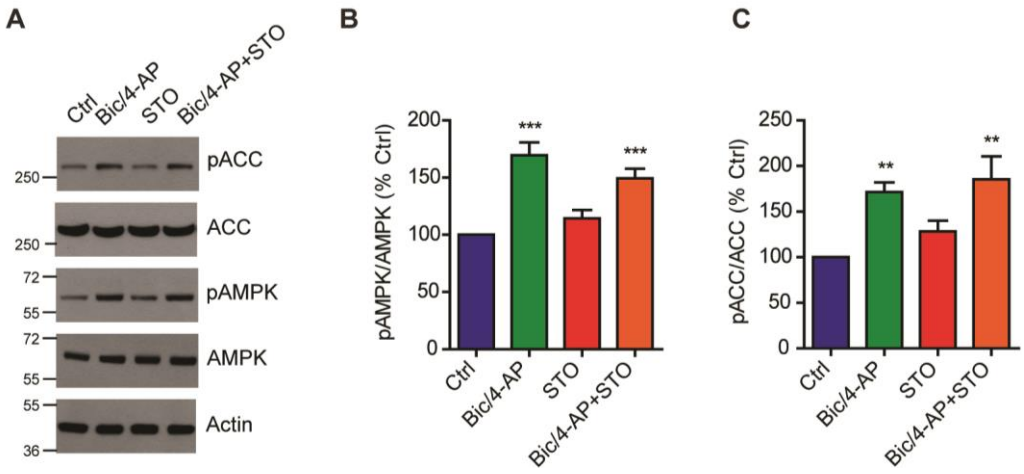


**Figure S2 - SA induced activation of AMPK is not mediated by CaMKKβ.** Related to Figure 1.

(**A**) Primary neurons treated with Bic/4-AP (10 min) after 20 min pre-treatment or not with the CaMKKβ specific inhibitor STO-609 (STO, 10 µM) were subjected to immunoblotting with anti- phosphorylated AMPK and ACC, total AMPK and ACC, and Actin. Results are representative of at least 5 experiments. (**B-C**) Quantifications of WB as in A showing the ratios phosphorylated AMPK/total AMPK (pAMPK/AMPK) and phosphorylated ACC/total ACC (pACC/ACC) expressed as percentage of control (n=5).

Results show mean ± SD. One-way ANOVA followed by Bonferroni's post-test was used for evaluation of statistical significance. * $p < 0.05$, ** $p < 0.01$, *** $p < 0.001$.

**Figure S3**

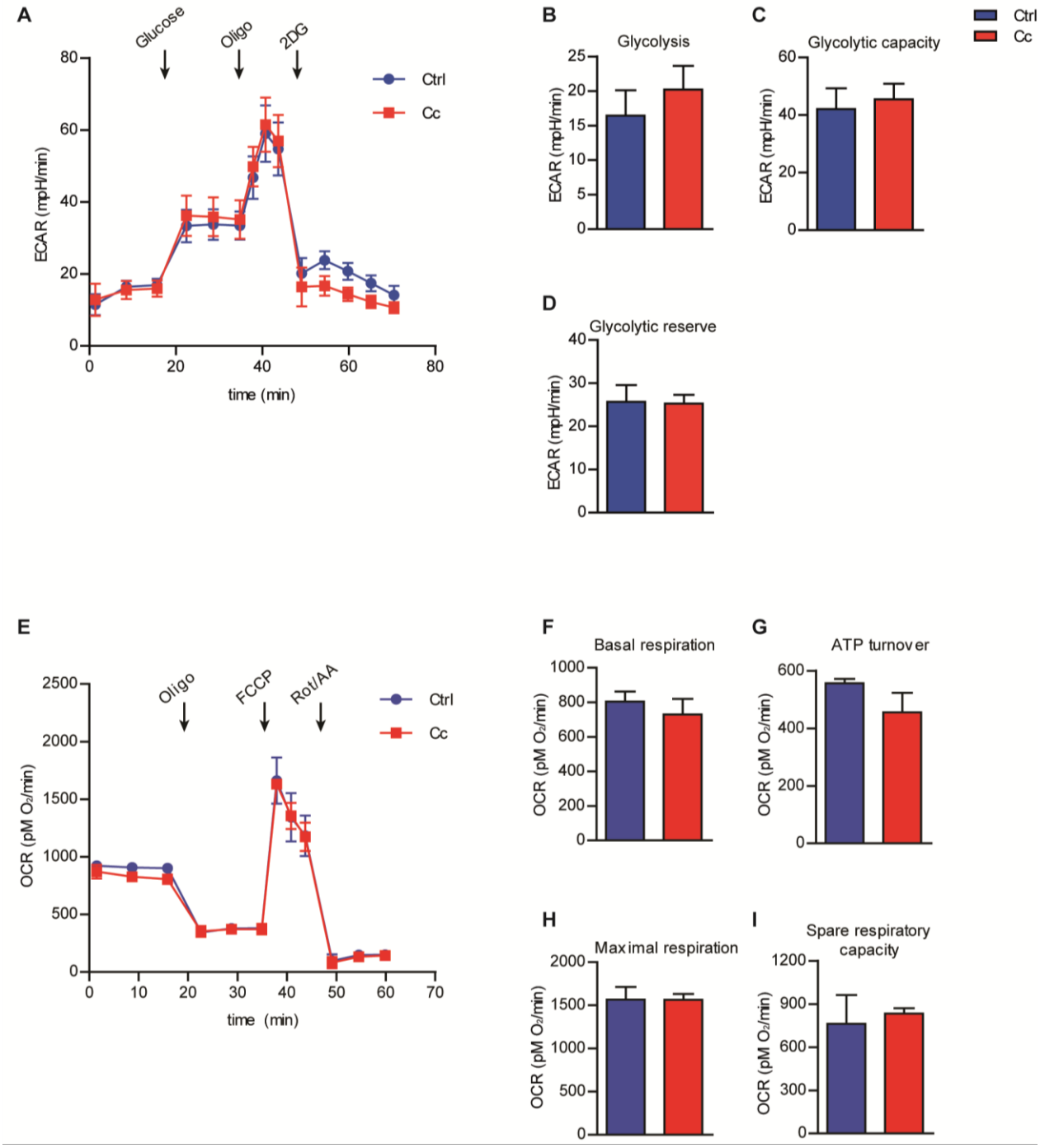


**Figure S3 - Effect of Compound C on glycolytic and mitochondrial oxidative phosphorylation profiles in primary neurons.** Related to Figure 2.

(**A-I**) Extracellular acidification rate (ECAR, A) and oxygen consumption rate (OCR, E) measured using the Seahorse technology in the presence or absence of the AMPK inhibitor Compound C (Cc, 10 μM). (A) ECAR profile is monitored under basal conditions and upon the sequential injection of saturating concentration of glucose, Oligo and 2DG as indicated by arrows. (E) OCR profile monitored under basal condition and following the sequential injection of Oligo, FCCP, and Rot/AA as indicated by the arrows. ECAR and OCR are indicators of glycolysis and mitochondrial respiration, respectively. (B) Basal glycolysis, (C) glycolytic capacity, and (D) spare glycolytic reserve expressed as mpH/min. (F) Basal respiration, (G) ATP turnover stimulation, (H) maximal respiration, and (I) spare respiratory capacity expressed as pM $O_2$/min. Results are representative of at least 3 independent experiments.

Results show mean ± SD. One-way ANOVA (B-D, F-I) followed by Bonferroni's post-test were used for evaluation of statistical significance. * $p < 0.05$, ** $p < 0.01$, *** $p < 0.001$.

**Figure S4**

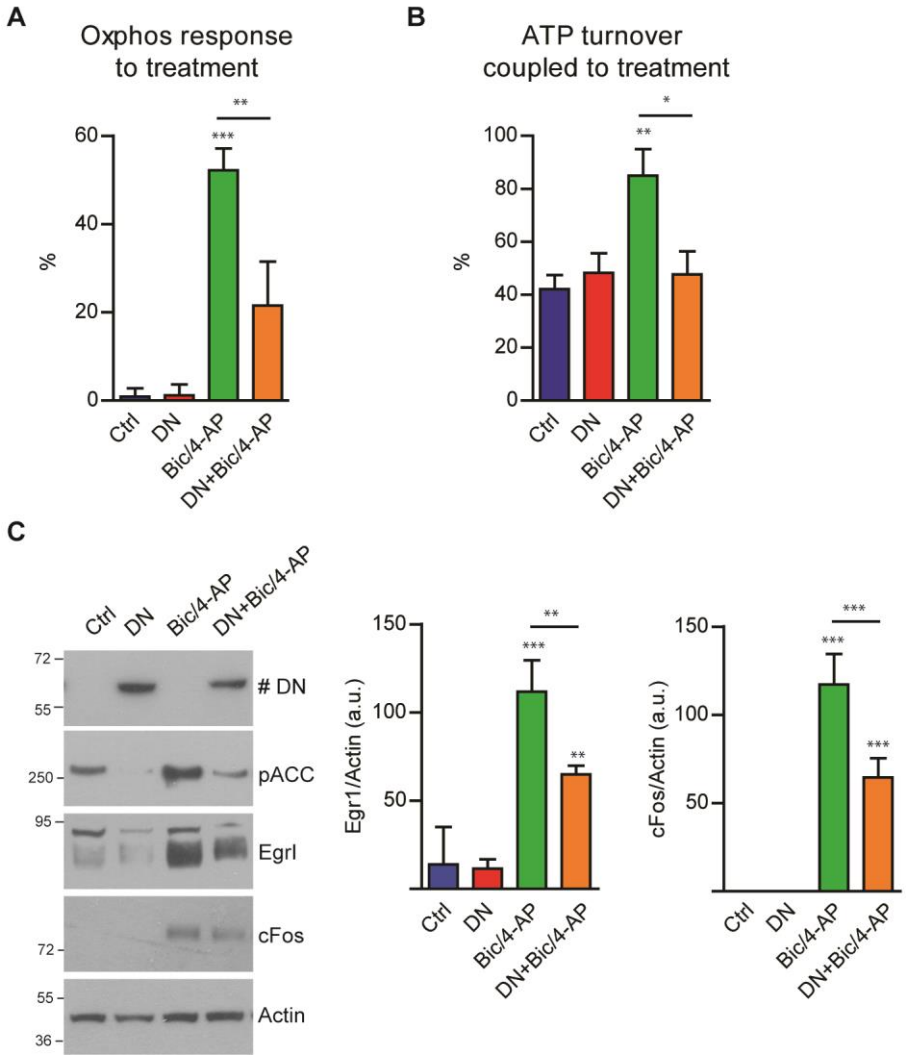


**Figure S4 – AMPK inhibition using a dominant negative construct repress the metabolic response to SA and the expression of IEGs.** Related to Figure 2 and Figure 4.

(**A-B**) OCR response to treatment (A) and ATP turnover after treatment (B) were evaluated using the Seahorse technology in primary neurons expressing a dominant negative (DN) form of AMPK. Results are expressed as percentage of the first respiration point (n=3). (**C**) Immunoblotting with anti-myc (# DN labels the overexpressed DN-AMPK construct), Egrl, cFos, and Actin in lysates obtained from 15 DIV neurons stimulated with Bic/4-AP for 2 hr, 4 days after infection with DN-AMPK. Results are representative of 3 experiments. Quantification of WB showing the expression of the IEGs Egrl and cFos (n=3).

Results show mean ± SD. One-way ANOVA followed by Bonferroni's post-test was used for evaluation of statistical significance. * $p < 0.05$, ** $p < 0.01$, *** $p < 0.001$.

**Figure S5**

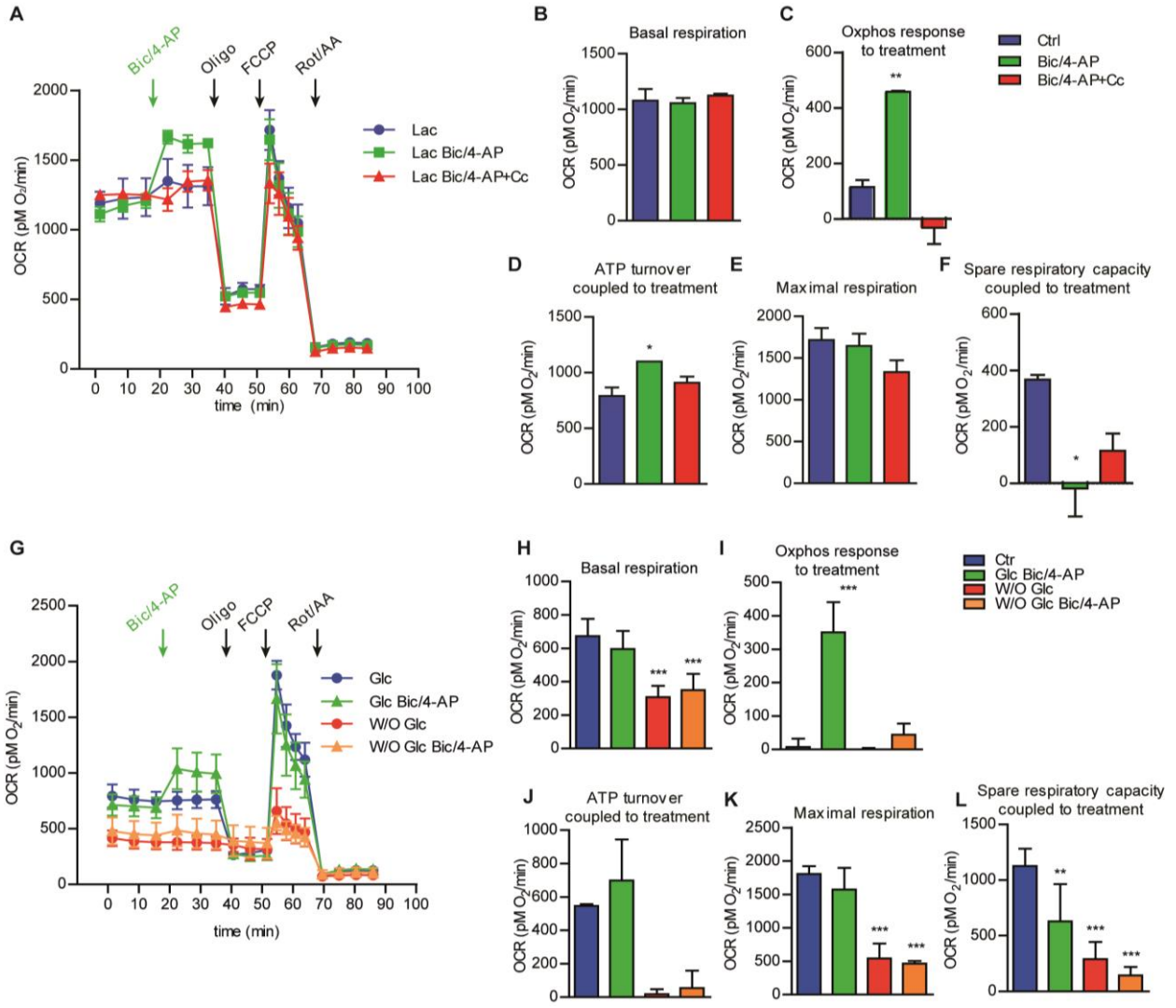


**Figure S5 – Utilization of mitochondrial alternative substrates by primary neurons in response to SA.** Related to Figure 2 and Figure 3.

(**A**) Oxygen consumption rate (OCR) measured using the Seahorse technology after Bic/4-AP stimulation (green arrows) in the presence or absence of L-Lactate (Lac, 10 mM). OCR profile was monitored under basal conditions and following the sequential injection of assay medium, in Ctrl group, or Bic/4-AP, in the stimulated groups, Oligo, FCCP, and Rot/AA as indicated by the arrows. (**B-F**) Basal respiration (B), oxphos response to treatment (C), ATP turnover after treatment (D), maximal respiration (E), and spare respiratory capacity after treatment expressed as pM $O_2$/min (F). (**G-L**) Oxygen consumption rate (OCR, G) measured using the Seahorse technology after Bic/4-AP stimulation (green arrows) in the presence (Glc, 10 mM) or

absence (W/O Glc) of glucose. OCR profile was monitored under basal conditions and following the sequential injection of assay medium, in Ctrl group, or Bic/4-AP, in the stimulated groups, Oligo, FCCP, Rot/AA as indicated by the arrows. (H) Basal respiration, (I) oxphos response to treatment, (J) ATP turnover after treatment, (K) maximal respiration, and (L) spare respiratory capacity after treatment expressed as pM $O_2$/min.

Results are representative of at least 3 independent experiments and show mean ± SD. One-way ANOVA followed by Bonferroni's post-test was used for evaluation of statistical significance. * $p < 0.05$, ** $p < 0.01$, *** $p < 0.001$.

**Figure S6**

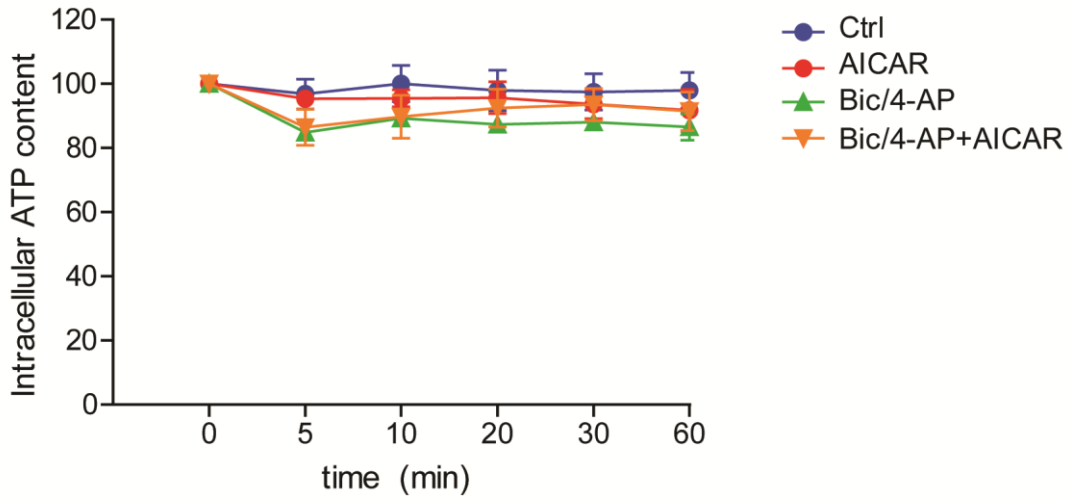


**Figure S6 – Intracellular ATP levels following Bic/4-AP stimulation in AICAR pre-treated neurons.** Related to Figure 5.

Intracellular ATP levels in neurons pre-treated or not with AICAR (24h, 1mM) and stimulated or not with Bic/4-AP for the indicated times (n=3-4). Results show mean ± SD, values are expressed as percentage of ATP at time 0.

**Figure S7**

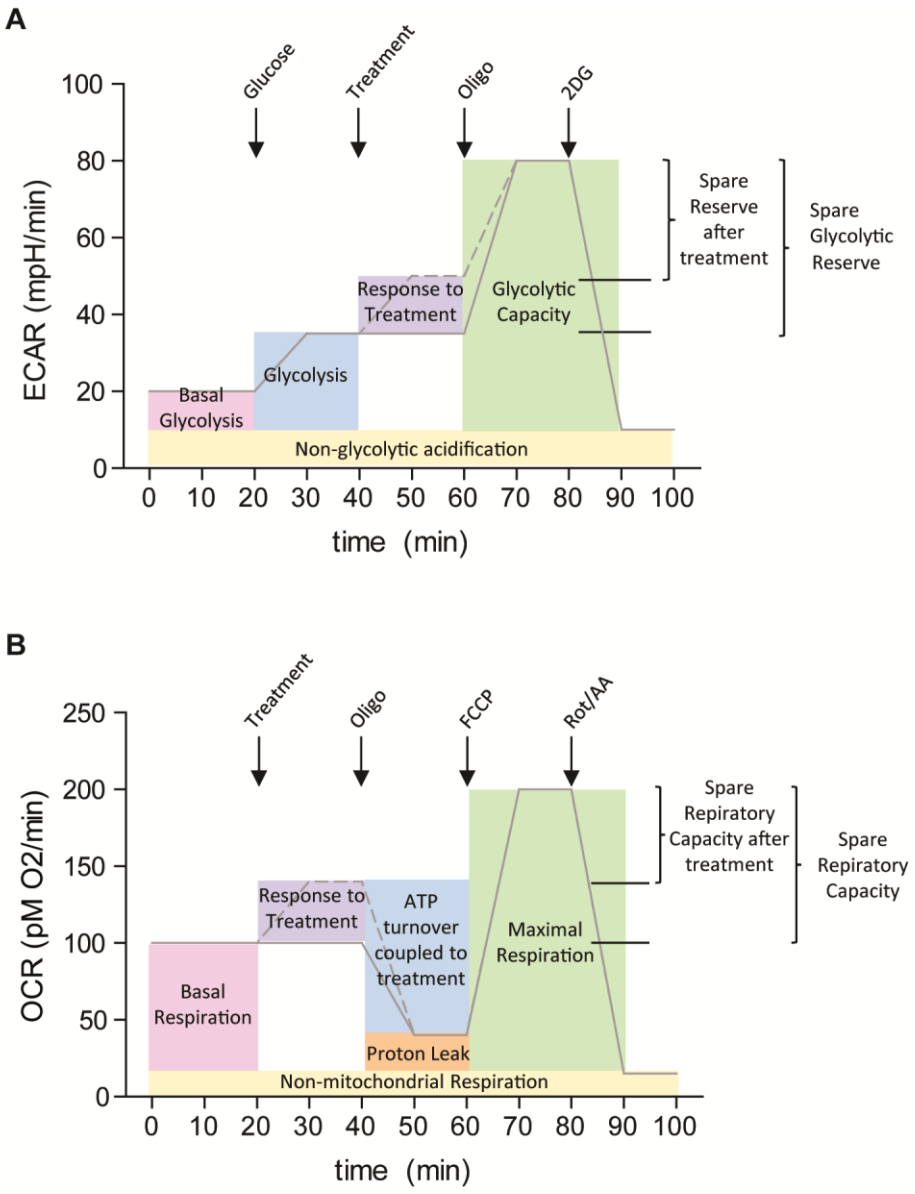


**Figure S7 – Schematic representation of metabolic parameters calculated via the Seahorse assay.** Related to Figure 2, Figure 5, Figure S3, Figure S4 and Figure S5.

Schematic representation of glycolytic and mitochondrial respiration profile obtained using Seahorse XFe24 respirometry and corresponding metabolic parameters. (**A**) The extracellular acidification rate (ECAR in mpH/min), reflects the intracellular glycolytic flux. Glycolytic flux is monitored in basal conditions as well as during the sequential injection of saturating glucose, treatment, oligomycin (Oligo) and 2-deoxy-D-deoxyglucose (2DG), as indicated by arrows. Glycolysis is calculated as the ECAR value difference before and after glucose injection. Response to Treatment is the maximal ECAR difference before and after

treatment injection. Glycolytic Capacity is calculated as the difference in ECAR between the Non-glycolytic acidification, induced by 2DG injection, and the maximal ECAR value after Oligo injection. Spare glycolytic Reserve is the ECAR difference between Glycolytic Capacity and Glycolysis. Spare Reserve after treatment is the difference between Glycolytic Capacity and Response to Treatment. (**B**) Mitochondrial respiration is expressed in oxygen consumption rate (OCR in $pMO_2$/min). Mitochondrial respiration is monitored in basal condition as well as during the sequential injection of treatment, oligomycin (Oligo), FCCP and rotenone/antimycin A (Rot/AA). Basal Respiration is obtained as the difference of between the respiration of unstimulated cell, at the beginning of the test, and the OCR value after Rot/AA injection (Non-mitochondrial Respiration). Response to treatment is calculated as the maximal OCR increase in response to treatment injection compared to the OCR at Basal Respiration. ATP turnover after treatment is the difference between the maximal OCR at response to Treatment and minimal OCR value after Oligo injection. Proton leak is difference between the lower OCR value after Oligo injection and Non-mitochondrial respiration. Maximal Respiration is the difference in OCR between the maximal OCR value after FCCP injection and the Non-mitochondrial respiration that is obtained after Rot/AA injection. Spare Respiratory Capacity is the OCR difference between the Maximal Respiration and the Basal Respiration. Spare Respiratory Capacity after treatment is calculated as the difference between the Maximal Respiration and the maximal Response to Treatment.

**Transparent Methods**

*Chemicals and reagents / antibodies*

Oligomycin, Carbonyl cyanide-4-(trifluoromethoxy)phenylhydrazone (FCCP), Antimycin A (AA), Rotenone (Rot), 4-Amynopyridine (4-AP), L-Lactate (Lac), iodoacetate and sodium pyruvate (NaPyr) were purchased from Sigma, 2-deoxy-D-glucose (2DG) from Acros, Compound C (Cc) from Santa Cruz, Bicuculline (Bic), MK-801, NBQX, STO-609, N1-(β-D-Ribofuranosyl)-5-aminoimidazole-4-carboxamide (AICAR) and Metformine from Tocris, Glucose 20% solution was purchased from Invitrogen. Antibodies directed against AMPKα, ACC, phospho-Ser$^{79}$ACC, ERK1/2, phospho-Thr$^{202}$/Tyr$^{204}$ERK1/2, phospho-Thr$^{581}$MSK, phospho-Thr$^{380}$p90RSK and phospho-Ser$^{133}$CREB were obtained from Cell Signaling technology. Anti phospho-Thr$^{172}$AMPKα, Arc, cFos, and EgrI antibodies were from Santa-cruz. Anti-Actin antibody was from BD Transduction Laboratory.

*Animals*

All animal experiments were performed according to procedures approved by the local Animal Ethical Committee following European standards for the care and use of laboratory animals (agreement APAFIS#4689-2016032315498524 v5 from CEEA75, Lille, France).

*Surgical procedures and injections*

Three-month-old male C57BL/6J mice were obtained from the Jackson Laboratory. Bilateral hippocampal surgeries were performed as described by Brouillette et al (Brouillette et al., 2012). Briefly, bilateral cannulae (328OPD-2.8/Spc with a removable dummy wire; Plastics One) were stereotaxically implanted into the hippocampus (coordinates with respect to bregma: -2.2 mm anteroposterior [AP], +/- 1.4 mm mediolateral [ML], -2.1 mm dorsoventral [DV], according to the Paxinos and Franklin mouse brain atlas) in anesthetized mice (100 mg/kg of ketamine and 10 mg/kg of xylazine, i.p.). After surgery, the animals recovered for 10 days before undergoing any procedures. After 10 days of recovery, awake and freely moving mice were injected once with 2 µl of Compound C or an equal volume of vehicle buffer at a rate of 0.25 µl/min via cannulae PE50 tubing (Plastics One) connected to a 10 µL Hamilton syringe pump system (KDS310; KD Scientific). The cannulae was capped to prevent reflux of the injected solution.

*Inhibitory avoidance*

Ten days after the surgery, mice underwent the inhibitory avoidance (IA) paradigm. Control mice (Saline) were injected with saline solution (0.9 % NaCl) while the treated mice were injected with Compound C (2 µl at 100 µM in saline) 20 min before running the acquisition test (Acq). The IA apparatus consisted in a rectangular shaped box that is divided into a safe illuminated compartment and a dark shock compartment. During the Acq session, each mouse was placed in the safe compartment and allowed to access the dark chamber where a brief foot shock (0.3 mA, 2 s) was delivered. The mouse was left in the dark compartment for one minute, before being replaced in its home cage. Latency to enter the shock compartment was taken as a measure of acquisition (Acq). 24 hr later, a retention test (Test 1) was run. In this phase, each mouse was placed in the light chamber and the latency to enter the dark compartment was recorded, however no foot shock was delivered when the mouse entered the dark chamber. A second test was run 6 days after the acquisition test (Test 2) in order to assess memory retention. To verify the ability of the injected mice to make new long term memory, each injected mouse underwent a second acquisition test 7 days after the first one (Retraining), and retention was tested 24 hr after (Test 3).

*Extracellular long-term recordings in the CA1-region of the hippocampus*

Mice were killed by cervical dislocation and hippocampal slices prepared from the dorsal area of the right hippocampus as reported previously (Ahmed et al., 2015; Denayer et al., 2008). In brief, the right hippocampus was rapidly dissected out into cold (4$^{o}$C) artificial cerebrospinal fluid (ACSF), saturated with carbogen (95% $O_2$/5% $CO_2$). ACSF consisted of 124 NaCl, 4.9 KCl, 25.6 $NaCO_3$, 1.20 $KH_2PO_4$, 2.0 $CaCl_2$, 2.0 $MgSO_4$, and 10.0 glucose (in mM), adjusted to pH 7.4. Transverse slices (400 µm thick) were prepared from the dorsal area of the right hippocampus with a tissue chopper and placed into a submerged-type chamber, where they were kept at 32$^{o}$C and continuously perfused with ACSF at a flow-rate of 2.2 ml/min. After 90 min incubation, one slice was arbitrarily selected and a custom-made tungsten electrode was placed in CA1 stratum radiatum for stimulation in constant current mode. For recording of field excitatory postsynaptic potentials (fEPSPs), a glass electrode (filled with ACSF, 3-7 MΩ resistance) was placed in the stratum radiatum. The time course of the field EPSP (fEPSP) was measured as the descending slope function for all sets of experiments. After a further hour of incubation, input/output curves were established and the stimulation strength was adjusted to elicit a fEPSP-slope of 35% of the maximum and was kept constant throughout the experiment. During baseline recording, three single stimuli (0.1 ms pulse width; 10 s interval) were measured every 5 min and averaged. A robust LTP was induced by three theta

burst stimuli (TBS), separated by 10 min. Compound c (Cc) was applied from 30 minutes prior to until 30 min after the first TBS. To allow for direct comparisons all experiments were interleaved between the experimental and control group. Intergroup differences in LTP were examined using ANOVA with repeated measures (RM-ANOVA, SPSS 19). For intragroup comparisons, Wilcoxon's matched-pairs signed-rank test was employed (SPSS 19). Group differences at single time points were tested using the Welch-test.

*Primary Neuronal Culture*

Primary neurons were prepared as previously described (Domise et al., 2016). Briefly, foetuses at stage E18.5 were obtained from pregnant C57BL/6J wild-type female mice (The Jackson Laboratory). Forebrains were dissected in ice-cold dissection medium composed of Hanks' balanced salt solution (HBSS) (Invitrogen) supplemented with 0.5 % w/v D-glucose (Sigma) and 25 mM Hepes (Invitrogen). Neurons were dissociated and isolated in ice-cold dissection medium containing 0.01 % w/v papain (Sigma), 0.1 % w/v dispase (Sigma), and 0.01 % w/v DNaseI (Roche) and by incubation at 37 °C for 15 min. Cells were spun down at 220 x g for 5 min at 4°C, resuspended in Neurobasal medium supplemented with 2% B27, 1 mM NaPyr, 100 units/ml penicillin, 100 µg/ml streptomycin, 2 mM Glutamax (Invitrogen), and plated at a density of $6*10^6$ cells/plate. Fresh medium was added every 3 days (1:3 of starting volume). Cells were then treated and collected between DIV 14-17.

*Construct and production of lentiviral vectors*

N-terminally myc-tagged wild-type (wt) and K45R mutated AMPK$\alpha$2 rat sequences were subcloned from Addgene plasmids 15991 and 15992 (Mu et al., 2001) into pENTR/D backbone using the In-Fusion HD cloning kit (Clontech) with the following primers: Fwd: 5'-CACCATGGTGCGGGGTTCTCAT and Rev-Trunc: 5'-GTCACCCTAGTATAAACTGTTCATCAC for the wtAMPK$\alpha$2 and Rev: 5'-TCAACGGGCTAAAGCAGTGATA for the K45R-AMPK$\alpha$2 to obtain respectively a constitutive active (CA) truncated form of AMPK ending at position 312, the AMPK$\alpha$2(1-312)-pENTR/D, and a kinase dead dominant negative (DN) form of AMPK, the AMPK$\alpha$2K45R-pENTR/D. Subsequently, pENTR/D vectors were recombined with SIN-PGK-cPPT-RFA-WHV lentiviral vectors using the Gateway LR Clonase II enzyme (Thermo Fisher) to obtain AMPK$\alpha$2(1-312)-pLenti and AMPK$\alpha$2K45R-pLenti constructs. The production of lentiviral vectors (LV) batches was as previously described (Caillierez et al., 2013). Primary neurons were infected with LV at 10 DIV and were used for experiments 4 days after LV infections.

*Intracellular ATP quantification*

Intracellular ATP content was quantified using the Dual-Glo® Luciferase Assay System (Promega), according to the supplier's instructions. Briefly, after treatments, primary neurons were incubated with the Dual- Glo® substrate for 10 min at RT before assessing luciferase activity using Spectramax® i3 (Molecular Devices).

*Phospho-Kinase array*

For the phospho-kinase assay, the array membranes were incubated with cell lysates (250 µg of total proteins per array) and subsequently processed according to the manufacturer's instructions (R&D Systems).

*Seahorse assay*

For Seahorse XFe24 respirometry assay, 100,000 neuronal cells were seeded in each well. The assay medium was composed of Dulbecco's Modified Eagle Medium base (DMEM, D-5030 Sigma) supplemented with 2 mM L-Glutamine (Invitrogen), 1.85 g/l NaCl (VWR), 3 mg/l Phenol Red (Sigma) and adjusted to pH 7.3+/-0.05. For each assay, cells were rinsed with the assay medium before being pre-incubated at 37°C without $CO_2$ 20 min prior the reading. For the glycolytic test, the extracellular acidification rate (ECAR in mpH/min) was monitored during basal condition (the mixing 2:30 min, waiting 2:00 min, reading 2:30 min cycle was repeated three times) and upon the sequential addition of saturating concentration of Glucose (10 mM) (the mixing 2:30 min, waiting 2:00 min, reading 2:30 min cycle was repeated 3 times), followed by Bic/4-AP (50 µM/2.5 mM) (the mixing 1:00 min, waiting 1:00 min, reading 2:30 min cycle was repeated five times), oligomycin (Oligo 1 µM) (the mixing 2:30 min, waiting 2:00 min, reading 2:30min cycle was repeated two times), and 2DG (150 mM) (the mixing 2:30 min, waiting 2:00 min, reading 2:30 min cycle was repeated two times). Glycolysis was expressed as ECAR increase after glucose addition. The glycolytic response to Bic/4-AP was calculated as the ECAR difference before and after the injection of Bic/4-AP, glycolytic capacity was calculated as the maximum ECAR reached following oligomycin injection when compared to basal conditions before glucose injection, glycolytic reserve as the difference between ECAR increase after oligomycin addition and upon glucose injection. The spare glycolytic reserve after Bic/4-AP injection was calculated as the percentage of the glycolytic reserve spared upon response to Bic/4-AP

treatment. In the mitochondrial stress test, the oxygen consumption rate (OCR in $pMO_2$/min) was monitored during the basal condition (the mixing 1:30 min, waiting 2:00 min, reading 3:00 min cycle was repeated three times) and after the subsequent injection of Bic/4-AP (50 µM/2.5 mM) (the mixing 1:30 min, waiting 2:00 min, reading 2:00 min cycle was repeated three times), oligomycin (Oligo, 1 µM) (the mixing 1:20min, waiting 1:20min, reading 2:00min cycle was repeated three times), FCCP (0.5 µM) (the mixing 0:20 min, waiting 0:00 min, reading 2:00 min cycle was repeated four times), Rotenone/Antimycin A (Rot/AA 1 µM/1 µM) (the mixing 1:20 min, waiting 1:20 min, reading 2:00 min cycle was repeated three times). For mitochondrial stress test, the assay medium was supplemented with glucose (10 mM), or L-Lactate (10 mM), or NaPyr (10 mM), as specified, before the pre-incubation without $CO_2$. Basal respiration was expressed as the difference in OCR before Bic/4-AP and after Rot/AA injection. The oxphos response to Bic/4-AP was expressed as the increase of OCR before and after Bic/4-AP addition. ATP turnover after Bic/4-AP treatment was calculated as the OCR difference before and after oligomycin injection. Maximal respiration was calculated as the OCR increase after FCCP compared to OCR upon Rot/AA injection, while spare respiratory capacity was expressed as the increase in OCR after FCCP when compared to basal respiration OCR level. Spare respiratory capacity after Bic/4-AP treatment was calculated as the percentage of mitochondrial OCR spare respiratory capacity after Bic/4-AP injection. Graphical explanation of each of the measurements is depicted in Figure S7. The pH of the drug solutions were adjusted to pH 7.3+/-0.05 prior to their use.

*Metabolomics analysis*

Five hundred thousand neurons were supplemented with media containing uniformly labelled $^{13}$C-glucose (25 mM) for 30 min. Cells were rinsed with ice-cold 0.9% NaCl solution and metabolites were extracted by adding 250 µl of a 50-30-20 solution (methanol-acetonitrile-10 mM tris HCl pH 9.4) to the cells. Plates were then incubated for 2-3 min on ice. Cells were scraped and transferred to an eppendorf tube before centrifugation at 20,000 x g for 10 min at 4°C, supernatants were then transferred to a fresh tube and stored at -80°C. Separation of metabolites prior to Mass Spectrometry (MS) measurement was performed using a Dionex UltiMate 3000 LC System (Thermo Scientific) coupled to a Q Exactive Orbitrap mass spectrometer (Thermo Scientific) operating in negative ion mode. Practically, 15 µl of the cellular extract was injected on a C18 column (Aquility UPLC®HSS T3 1.8µm 2.1x100mm) and the following gradient was performed by solvent A ($H_2O$, 10mM Tributyl-Amine, 15mM acetic acid) and solvent B (100% Methanol). Chromatographic separation was achieved with a flowrate of 0.250ml/min and the following gradient

elution profile: 0min, 0%B; 2min, 0%B; 7min, 37%B; 14min, 41%B; 26min, 100%B; 30min, 100%B; 31min, 0%B; 40min, 0%B. The column was placed at 40°C throughout the analysis. The MS operated both in full scan mode (m/z range: 70-1050) using a spray voltage of 4.9 kV, capillary temperature of 320°C, sheath gas at 50.0, auxiliary gas at 10.0. The AGC target was set at 3e6 using a resolution of 140.000, with a maximum IT fill time of 512 ms. Data collection was performed using the Xcalibur software (Thermo Scientific).

*Western blot (WB)*

For WB analysis, proteins from total cell lysates were separated in 8-16% Tris-Glycine gradient gels and transferred to nitrocellulose membranes. Membranes were then blocked in 5% fat-free milk in TBS-0.01% Tween-20, and incubated with specific primary antibodies overnight at 4 °C. Proteins were thereafter detected via the use of HRP-conjugated secondary antibodies and ECL detection system (ThermoFisher Scientific).

*Statistical analysis*

All statistical analyses were performed using GraphPad Prism (Prism 5.0d, GraphPad Software Inc, La Jolla, CA, USA).

**References**


Ahmed, T., Blum, D., Burnouf, S., Demeyer, D., Buee-Scherrer, V., D'Hooge, R., Buee, L., and Balschun, D. (2015). Rescue of impaired late-phase long-term depression in a tau transgenic mouse model. Neurobiology of aging *36*, 730-739.

Brouillette, J., Caillierez, R., Zommer, N., Alves-Pires, C., Benilova, I., Blum, D., De Strooper, B., and Buee, L. (2012). Neurotoxicity and memory deficits induced by soluble low-molecular-weight amyloid-beta1-42 oligomers are revealed in vivo by using a novel animal model. The Journal of neuroscience : the official journal of the Society for Neuroscience *32*, 7852-7861.

Caillierez, R., Begard, S., Lecolle, K., Deramecourt, V., Zommer, N., Dujardin, S., Loyens, A., Dufour, N., Auregan, G., Winderickx, J.*, et al.* (2013). Lentiviral delivery of the human wild-type tau protein mediates a slow and progressive neurodegenerative tau pathology in the rat brain. Molecular therapy : the journal of the American Society of Gene Therapy *21*, 1358-1368.

Denayer, E., Ahmed, T., Brems, H., Van Woerden, G., Borgesius, N.Z., Callaerts-Vegh, Z., Yoshimura, A., Hartmann, D., Elgersma, Y., D'Hooge, R.*, et al.* (2008). Spred1 is required for synaptic plasticity and hippocampus-dependent learning. The Journal of neuroscience : the official journal of the Society for Neuroscience *28*, 14443-14449.

Domise, M., Didier, S., Marinangeli, C., Zhao, H., Chandakkar, P., Buee, L., Viollet, B., Davies, P., Marambaud, P., and Vingtdeux, V. (2016). AMP-activated protein kinase modulates tau phosphorylation and tau pathology in vivo. Scientific reports *6*, 26758.

Mu, J., Brozinick, J.T., Jr., Valladares, O., Bucan, M., and Birnbaum, M.J. (2001). A role for AMP-activated protein kinase in contraction- and hypoxia-regulated glucose transport in skeletal muscle. Molecular cell *7*, 1085-1094.